iScience

CellPress
OPEN ACCESS

Perspective

Perspectives on the application of layered MPX_3 materials (M: Transition metal, X: Chalcogen) in confined catalysis and energy applications

Yefei Guo,[1,*] Yuriy Dedkov,[2,*] and Elena Voloshina[3,*]
[1]School of Physics and Advanced Energy, Henan University of Technology, Zhengzhou, Henan 450001, P.R. China
[2]Center for Advanced Laser Techniques, Institute of Physics, 10000 Zagreb, Croatia
[3]Division of Theoretical Physics, Ruđer Bošković Institute, 10000 Zagreb, Croatia
*Correspondence: yefeiguo@haut.edu.cn (Y.G.), ydedkov@ifs.hr (Y.D.), elena.voloshina@irb.hr (E.V.)
https://doi.org/10.1016/j.isci.2026.114702

SUMMARY

The concept of confined catalysis, where reactions occur within nanoscale environments that modulate reaction energetics, has emerged as a powerful paradigm for designing advanced catalytic systems. Inspired by the efficiency of enzyme active pockets through metal-enzyme cascade reactions, confined architectures provide unique opportunities to enhance activity and selectivity across a wide range of chemical processes. Here, layered transition metal phosphorus trichalcogenides (MPX_3, where M: transition metal and X: chalcogen) have attracted increased attention as versatile hosts for confined catalysis, where van der Waals gaps create natural nanoreactors stabilizing intermediates and hosting guest species. By coupling intrinsic catalytic activity with engineered confinement, MPX_3 materials offer new pathways toward efficient hydrogen storage, stable high-capacity batteries, and robust energy conversion systems. This perspective highlights the emerging role of MPX_3 compounds in confined catalysis and outlines the challenges and opportunities for their application in sustainable energy technologies.

INTRODUCTION

The global transition to sustainable energy systems strongly requires breakthroughs in the development of materials and systems that can drive efficient energy conversion, storage, and utilization.[1,2] Catalysis lies at the heart of this challenge, underpinning technologies from hydrogen production and CO_2 reduction to next-generation rechargeable batteries. Traditionally, catalyst development has focused primarily on engineering active sites through strategies such as compositional tuning, nanostructuring, and heterostructure formation.[3–5] Additionally, it is recognized that the microenvironment around these active sites can be important in dictating reactivity, selectivity, and long-term stability. Inspired by biological enzymes, where reactions occur in tailored pockets that stabilize intermediates and direct pathways,[6,7] the concept of *confined catalysis* has emerged as a powerful paradigm for heterogeneous catalysis.[8–11] In confined systems, nanoscale spaces alter adsorption energies, electronic states, and charge transfer, often enabling reaction pathways inaccessible in open environments.

Early examples of confinement were demonstrated in the pores of zeolites and metal-organic frameworks (MOFs),[12,13] or along the channels of carbon nanotubes (CNTs),[14,15] where natural spatial restrictions reshaped catalytic activity. However, the structural complexity and inhomogeneity of these systems often complicate mechanistic insights. Two-dimensional (2D) materials, in contrast, offer atomically defined and tunable confined spaces that can be systematically studied and engineered. For instance, the adsorption of small molecules such as CO on Pt surfaces is markedly weakened when a graphene or *h*-BN overlayer is present, with a measurable confinement energy that modifies both adsorption thermodynamics and reaction barriers.[16,17] Such studies revealed how confinement simultaneously imposes geometric constraints and modifies potential fields, creating microenvironments where catalytic activity can be selectively tuned.

The implications of this concept extend directly to *energy applications*, where confined catalysis has already been shown to dramatically affect performance. In the electrochemical hydrogen evolution reaction (HER), for example, nickel surfaces confined under graphene exhibit activity approaching that of platinum, arising from optimized hydrogen adsorption energies and improved charge transfer across the confined interface.[18,19] Similarly, confined environments have been demonstrated to accelerate CO_2 reduction[20] and oxygen reduction,[21] as well as to stabilize reaction intermediates that are otherwise short-lived in bulk systems. Beyond conversion, confinement plays a role in storage: nanoconfined hydrogen within 2D interlayers or porous shells displays altered binding enthalpies that are closer to the thermodynamic "sweet spot" for reversible hydrogen storage.[22–24] Confinement in van der Waals (vdW) gaps and layered architectures can thus provide pathways toward safer, denser, and more efficient hydrogen storage systems, addressing one of the grand challenges of a hydrogen economy.

Confined catalysis is also increasingly relevant to the operation of *batteries and supercapacitors*, where reaction microenvironments govern ion transport, electrode stability, and interfacial kinetics. In lithium-sulfur batteries, for instance, encapsulation strategies that confine polysulfides within nanoscale hosts suppress their diffusion and enhance cycle life.[25–27] Similarly, confinement of redox-active nanoparticles within porous or two-dimensional shells has been shown to stabilize interfaces against aggregation and side reactions, directly improving battery stability and capacity retention. Confinement also modifies the electrochemical potential landscape at electrode surfaces, lowering kinetic barriers and enhancing charge storage efficiency. These insights suggest that rationally designed confined architectures could become central to the future of high-performance electrochemical energy storage.

Taking into account the present-day demands and requests for materials for confined catalysis and energy applications, layered transition metal phosphorus trichalcogenides (MPX_3, M: transition metal, X: chalcogen) stand out as versatile and flexible platforms.[28–34] Their intrinsic properties, such as layered vdW structures, tunable band gaps, high tunability of electronic properties, and rich surface chemistry, make them attractive not only as catalysts for water splitting, CO_2 reduction, and oxygen evolution reactions (OERs), but also as hosts for confined reactions. The vdW gaps of MPX_3 can act as natural nanoreactors, trapping ions, molecules, or nanoparticles in well-defined environments, where adsorption and charge transfer can be finely tuned. This makes MPX_3 particularly relevant to confined hydrogen storage, as the interlayer spaces can modulate binding energies, and to battery electrodes, where encapsulation of active species within MPX_3 frameworks can stabilize cycling behavior. Encapsulation approaches developed in environmental catalysis, such as core-shell or yolk-shell structures, demonstrate how confinement improves selectivity, stability, and resistance to poisoning. These concepts can be directly extended to MPX_3 systems for energy storage and conversion. For instance, encapsulating redox-active nanoparticles in MPX_3-based shells could mitigate aggregation and dissolution in batteries, while simultaneously providing catalytic activity for conversion reactions. Similarly, embedding hydrogen within MPX_3 interlayers could exploit both confinement and transition-metal coordination effects, potentially leading to enhanced storage capacity and kinetics.

Overall, these considerations highlight confined catalysis as a unifying framework for tackling challenges in both energy conversion and storage. By harnessing nanoscale confinement, it is possible to tune adsorption, stabilize intermediates, and reshape reaction energetics in ways not achievable in open systems. Layered MPX_3 materials, with their unique combination of catalytic activity, electronic tunability, and intrinsic capacity to host confined environments, offer a promising frontier for this approach. This perspective aims to highlight the design principles and emerging opportunities for MPX_3-based confined catalysis, with particular attention to their potential roles in hydrogen storage and next-generation battery technologies. We will emphasize how confinement effects – geometric, electronic, and interfacial – can be harnessed within MPX_3 systems to unlock unique catalytic pathways. Finally, we outline the key challenges that must be addressed to fully exploit this material family in designing next-generation confined catalysts.

CONFINED REACTIONS

The design of catalytic materials has long been guided by the principle of exposing the maximum number of active sites to reactants, while maintaining stability and selectivity under working conditions. This traditional approach, however, encounters intrinsic limitations: the downsizing of nanoparticles to expose more surface atoms inevitably reduces stability due to sintering or poisoning, while open catalytic surfaces often suffer from undesired side reactions. The emergence of confined catalysis offers an alternative paradigm. By restricting catalytic processes within nanoscopic spaces, the energetics and kinetics of reactions can be modulated in ways that are impossible on extended surfaces. These confined environments generate specific microreactors, reminiscent of enzymatic pockets in biological systems, where the size, shape, and local electronic environment of the active site are precisely controlled.[6,7]

Several classes of materials naturally lend themselves to providing confined environments (Figure 1). Among these are (a) the vdW gaps in layered materials, (b) interfacial voids beneath 2D cover layers supported on substrates, (c) the one-dimensional channels of nanotubes, and (d) the cages or pores of zeolites and MOFs.[8,12,13,35–39] While these systems differ in dimensionality and chemical nature, they share the essential characteristic of spatial confinement, which endows them with unusual reactivity, enhanced selectivity, and often superior stability.

Layered materials, such as transition metal dichalcogenides, graphitic carbon nitride, and MXenes, offer vdW gaps between adjacent atomic layers that act as natural nanospaces (see examples in Figure 2).[40–46] The interlayer confinement modifies the charge distribution and electronic structure of both the host and guest species. In layered dichalcogenides, intercalated heteroatoms or small molecules can be stabilized within the gaps, where their electronic interaction with the surrounding lattice tunes their catalytic behavior. This principle has been used to explain improved HER activity when protons are reduced in nanoconfined environments between layers.[47] Moreover, nanoconfined fluids in such layered systems exhibit unusual properties: higher energy densities and enhanced ion transport compared to bulk electrolytes, making vdW gaps relevant not only for catalysis but also for energy storage applications[40] (Figure 2).

A related, but distinct platform for confinement arises at the interface between atomically thin cover layers and their supporting substrates. In these "under-the-carpet" geometries, first demonstrated with graphene and hexagonal boron nitride (*h*-BN) grown on metals, the confined space between the 2D sheet and the substrate traps reactants and intermediates. This geometry has been studied in detail by surface science methods, including ambient pressure photoelectron spectroscopy and *in situ* infrared spectroscopy, which allow direct observation of intercalated species.[8,35] One of the most striking examples comes from graphene-coated Pt(111) (Figure 3), where the adsorption energy of CO is reduced compared to

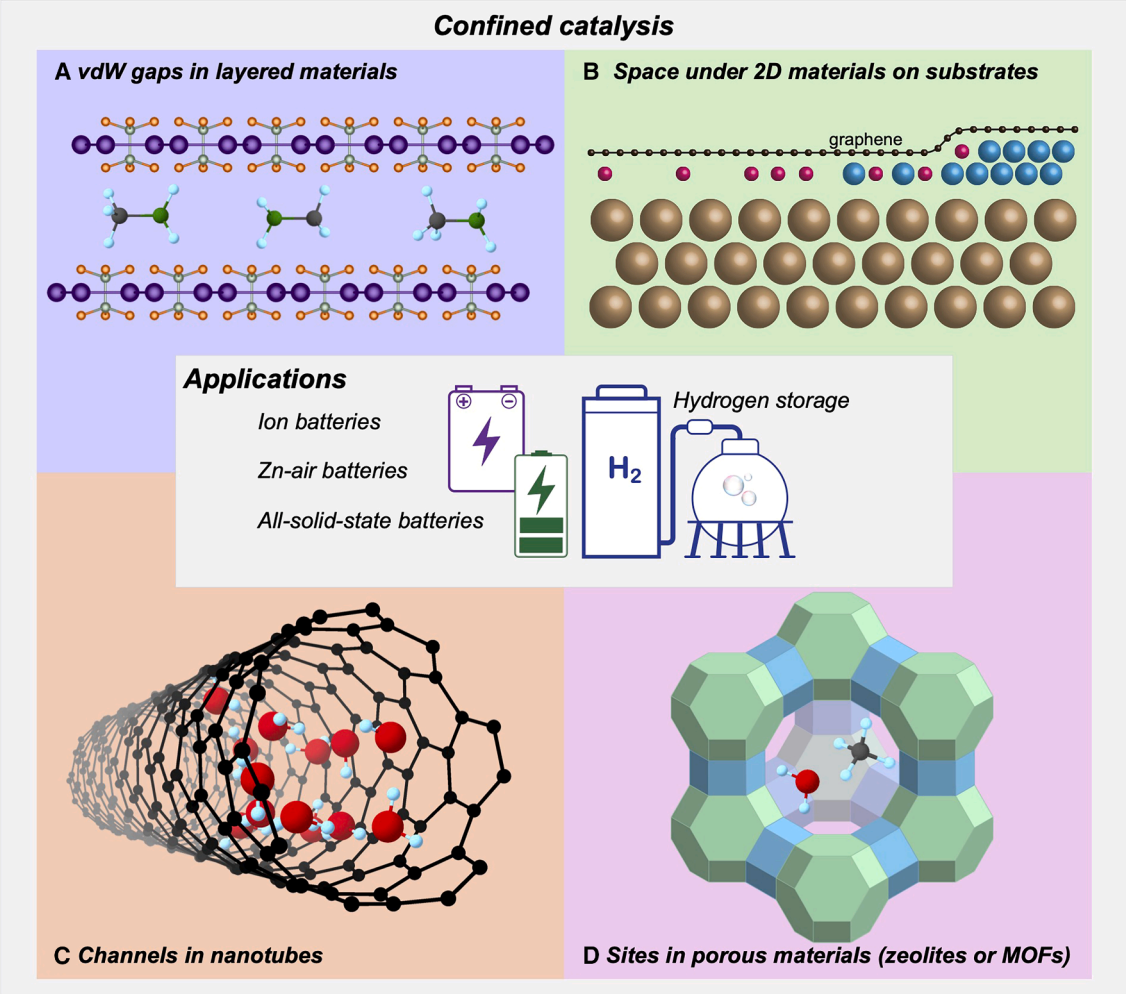

Figure 1. Materials for confined catalysis and energy storage applications

(A) vdW gaps in layered materials.

(B) Space under 2D materials on substrates.

(C) Channels in nanotubes.

(D) Active sites in porous materials.

the bare metal surface. As a result, CO oxidation proceeds with a lower activation barrier under the graphene cover, highlighting how a confined space can alter reaction energetics in a favorable direction.[16,48] Here, polar overlayers such as *h*-BN can induce stronger confinement fields compared to nonpolar graphene, owing to their stronger interaction with the metal substrate.

One-dimensional channels, most prominently those of carbon nanotubes, represent another archetype of confined catalysis. Nanotube interiors provide cylindrical confinement, where molecules experience restricted diffusion, unique adsorption geometries, and altered electronic coupling with active sites. Encapsulated metal clusters, such as Fe or Pt, within nanotube cavities, display modified *d*-band structures that shift adsorption energies of key intermediates.[49–51] For oxygen reduction reactions, these shifts translate into improved selectivity and lower overpotentials. Furthermore, the encapsulation of nanoparticles inside nanotubes prevents agglomeration, which is a major cause of catalyst deactivation in open systems. This stability enhancement is particularly relevant for high-temperature or electrochemical environments where sintering and poisoning are severe.

Porous materials such as zeolites and MOFs are perhaps the most established platforms for confined catalysis. Zeolites, with their crystalline microporous frameworks and strong Brønsted acid sites, have long been used in the petrochemical industry for cracking, isomerization, and hydrocarbon upgrading. The confinement in zeolite pores influences both enthalpic and entropic contributions to the activation free energy. The chemical flexibility of MOFs allows fine control of the pore environment, enabling the incorporation of catalytic centers either as metal sites within the framework or as functional groups in the linkers. Despite challenges related to stability and large-scale deployment, MOFs offer promising opportunities for confined catalysis in fine chemicals and pharmaceutical

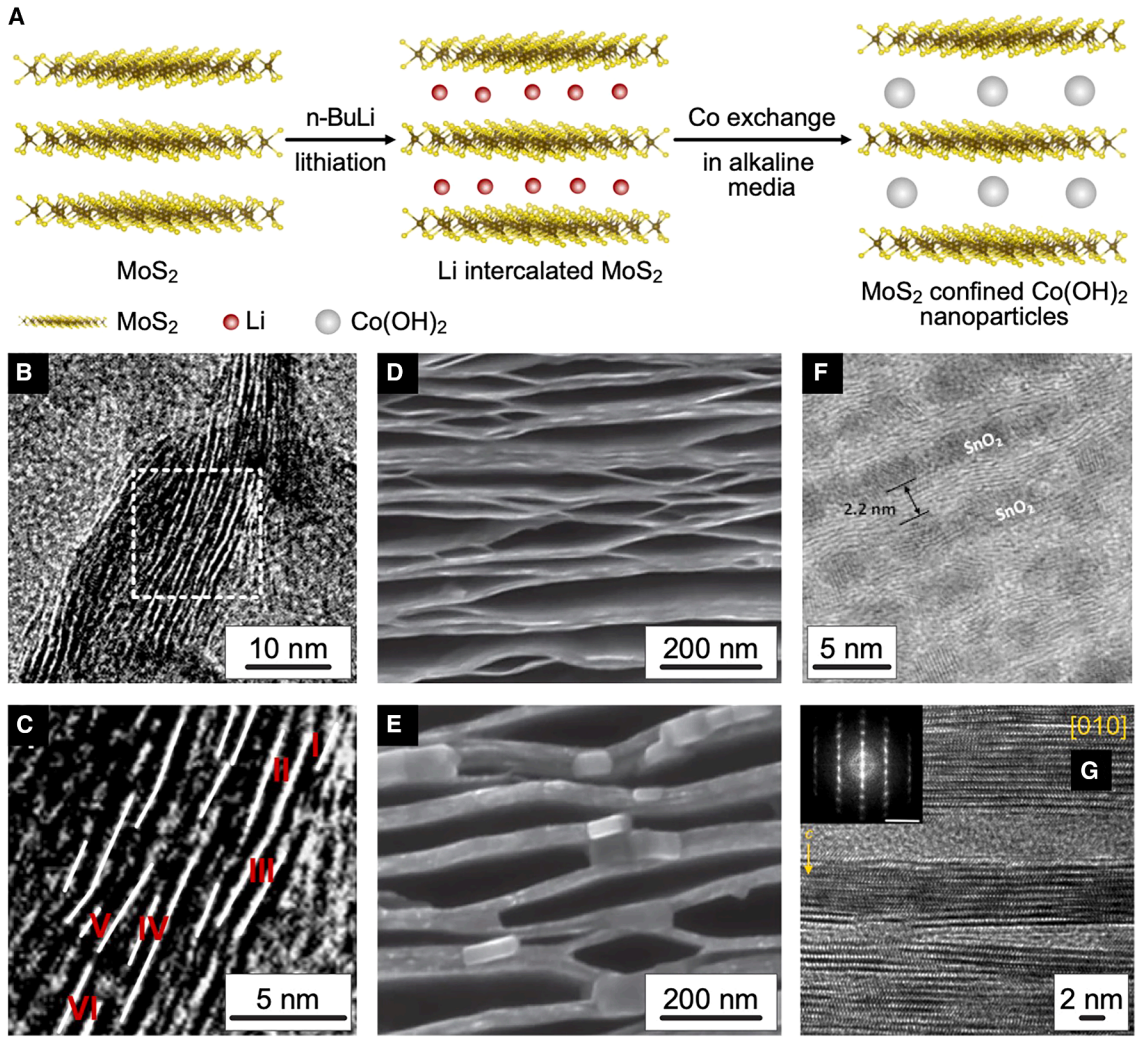

Figure 2. Examples of layered materials offering vdW gaps between adjacent atomic layers that act as natural nanospaces

(A) Scheme of synthesis of electrocatalysts for HER in alkaline media, consisting of $Co(OH)_2$ confined in MoS_2. Reproduced with permission.[40] Copyright 2018, American Chemical Society.

(B and C) Structural characterization of the Co-Ex-MoS_2 samples: HRTEM images of (B) the side view of the (002) planes and (C) an enlarged image. I, II, III, IV, and V in (C) indicate MoS_2 (002) planes with obviously different spacings. Reproduced with permission.[40] Copyright 2018, American Chemical Society.

(D and E) SEM images before (D) and after (E) intercalation of functionalized Ti_3C_2 with HM and DMF (24 h at 80°C), respectively. Reproduced with permission.[41] Copyright 2013, Springer Nature.

(F) HRTEM image of the ultramicrotomed cross-section of SGF. Reproduced with permission.[42] Copyright 2024, The Royal Society of Chemistry.

(G) HRTEM image of the specimen after EMIM intercalation with regions of crystalline $NiPS_3$ and amorphous regions. The inset shows the FFT of the corresponding HRTEM image. Reproduced with permission.[42] Copyright 2024, The Royal Society of Chemistry.

synthesis, where high selectivity is paramount. The strategy of encapsulation, more generally, has recently been highlighted as a way to achieve confinement even beyond naturally porous hosts using the core-shell catalysts, where nanoparticles are encapsulated in oxide shells such as TiO_2, SiO_2, or CeO_2[52] and hierarchical yolk-shell structures, where void spaces between the core and shell provide confined regions that act as nanoreactors, such as the porous TiO_2 shell decorated with Au-Pd nanoneedles.[53]

Taken together, these diverse platforms highlight the unifying concept that confined spaces – whether naturally occurring in layered structures, deliberately introduced under 2D materials, embedded in nanotube channels, or engineered in porous frameworks and core-shell architectures – provide unique chemical environments that differ fundamentally from open catalytic surfaces. The consequences of confinement include altered adsorption energies, modified charge transfer, stabilization of reactive intermediates, steric control over transition states, and enhanced resistance against deactivation. The growing body of evidence suggests that confined catalysis is not a niche effect, but rather a general strategy for designing next-generation catalysts across energy, environmental, and chemical sectors.

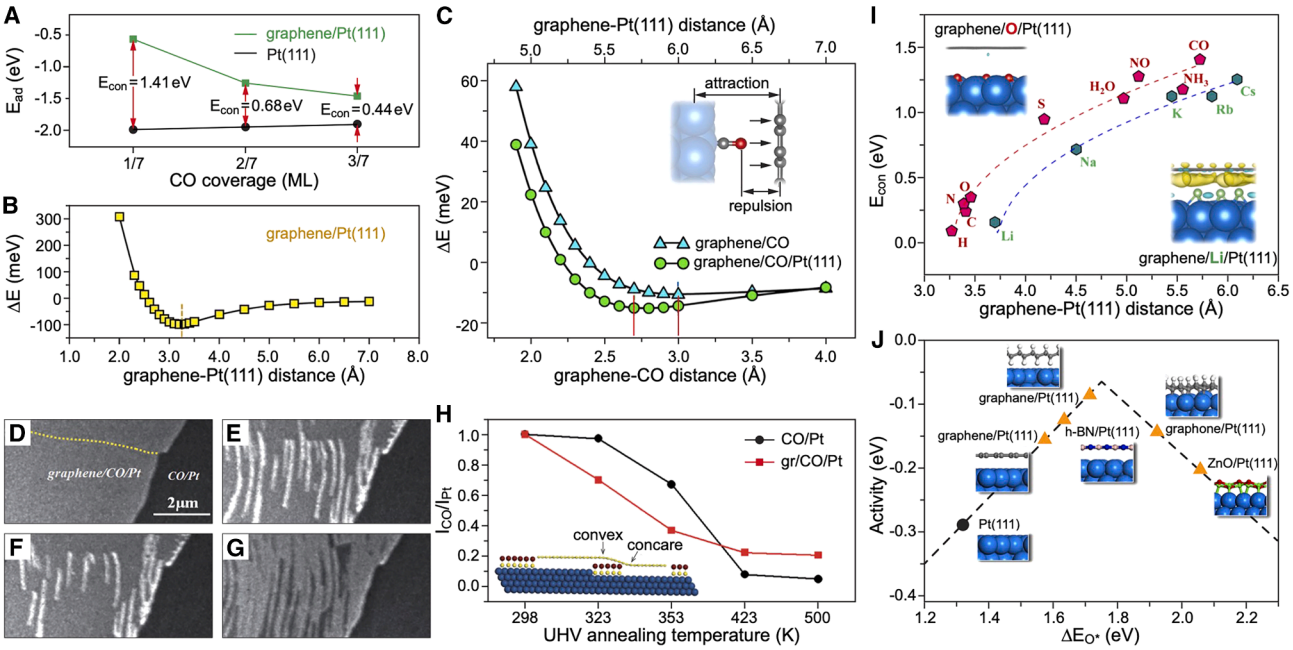

Figure 3. Confined catalysis in the "under-the-carpet" geometry

(A) Adsorption energies of CO on Pt(111) and graphene/Pt(111) and the derived confinement energies (E_{con}) with CO coverage at 1/7, 2/7, and 3/7 ML.

(B) Total energy differences of the graphene/Pt(111) system (averaged to each C atom of graphene) at each specific distance between graphene and Pt(111) surface relative to infinity.

(C) Total energy differences of the graphene/CO and graphene/CO/Pt(111) systems (averaged to each C atom of graphene) at each specific distance between graphene and CO relative to infinity. (Inset) Interaction between graphene layer, CO molecule, and Pt slab. Reproduced with permission.[16] Copyright 2017, National Academy of Sciences of the USA.

(D–F) LEEM images from the graphene/CO/Pt(111) surface kept in UHV and at room temperature for different times: (D) 0, (E) 200, (F) 402 s.

(G) Further annealing at 487 K in UHV. The dashed line in (D) marks the wrinkle location.

(H) XPS O 1*s* intensity of the CO-saturated Pt(111) surface and the CO-intercalated 0.7 ML graphene/Pt(111) surface annealed at various temperatures in UHV. The O 1*s* intensity was normalized by the Pt 4*f* intensity. Each annealing step lasted more than 10 min. The inset illustrates the desorption of CO molecules under graphene, except those trapped close to steps, at around room temperature. Reproduced with permission.[48] Copyright 2012, John Wiley and Sons.

(I) E_{con} for 1/7 ML nonmetal atoms and molecules (pink dots), as well as alkali metal atoms (green dots) in between graphene and Pt(111) with various graphene-Pt distance values. The pink dots and green dots are fitted in red and blue dashed lines, respectively. (Insets) Cross-section views of graphene/O/Pt(111) and graphene/Li/Pt(111) interfaces shown with electron density difference at the interface.

(J) The volcano curve relation between ORR activity and binding energies of O atoms (ΔE_{O^*}) on the Pt surface. (Insets) The interfacial structures. Reproduced with permission.[16] Copyright 2017, National Academy of Sciences of the USA.

INTERCALATION

Intercalation has become one of the most versatile strategies for engineering the properties of 2D materials and vdW heterostructures[54–58] (Figure 4). At its simplest, the process refers to the insertion of guest species into the interlayer spaces of layered crystals without destroying the strong in-plane covalently bonded structure. Moreover, beyond these structural changes, intercalation serves as a powerful tool to control charge density, tune interlayer interactions, and create new phases of the material with electronic, optical, or magnetic properties that are not accessible in the pristine parent materials. As emphasized in recent reviews, intercalation should be understood not as a static chemical transformation, but as a dynamic and multifunctional process that bridges synthetic chemistry, condensed matter physics, and device engineering.[56–58]

The aims of intercalation are multifold. One of the earliest and still most important drivers is the reversible storage of ions in electrode materials, exemplified by lithium intercalation in graphite (Figures 5A and 5B), which underpins modern battery technology.[54,56,61,62] Beyond energy storage, however, intercalation is pursued to achieve controlled modification of band structures and carrier densities (Figures 5C–5K), enabling the conversion of semiconductors into metals, the stabilization of superconducting states, or the manipulation of spin textures.[57] For example, Na and K intercalation in graphite leads to different staging behaviors and anisotropic transport compared to Li,[54] while $FeCl_3$ intercalation in graphene dramatically enhances its conductivity and transparency, making it useful for transparent electrodes.[63,64] By expanding the interlayer spacing, intercalation also facilitates exfoliation into monolayers and the synthesis of new heterostructures, providing a synthetic pathway complementary to mechanical or chemical exfoliation methods.[55,58,65,66] More recently, the insertion of organic molecules has extended these aims into the realm of hybrid architectures, where molecular functionality can be deliberately combined with inorganic layers to achieve

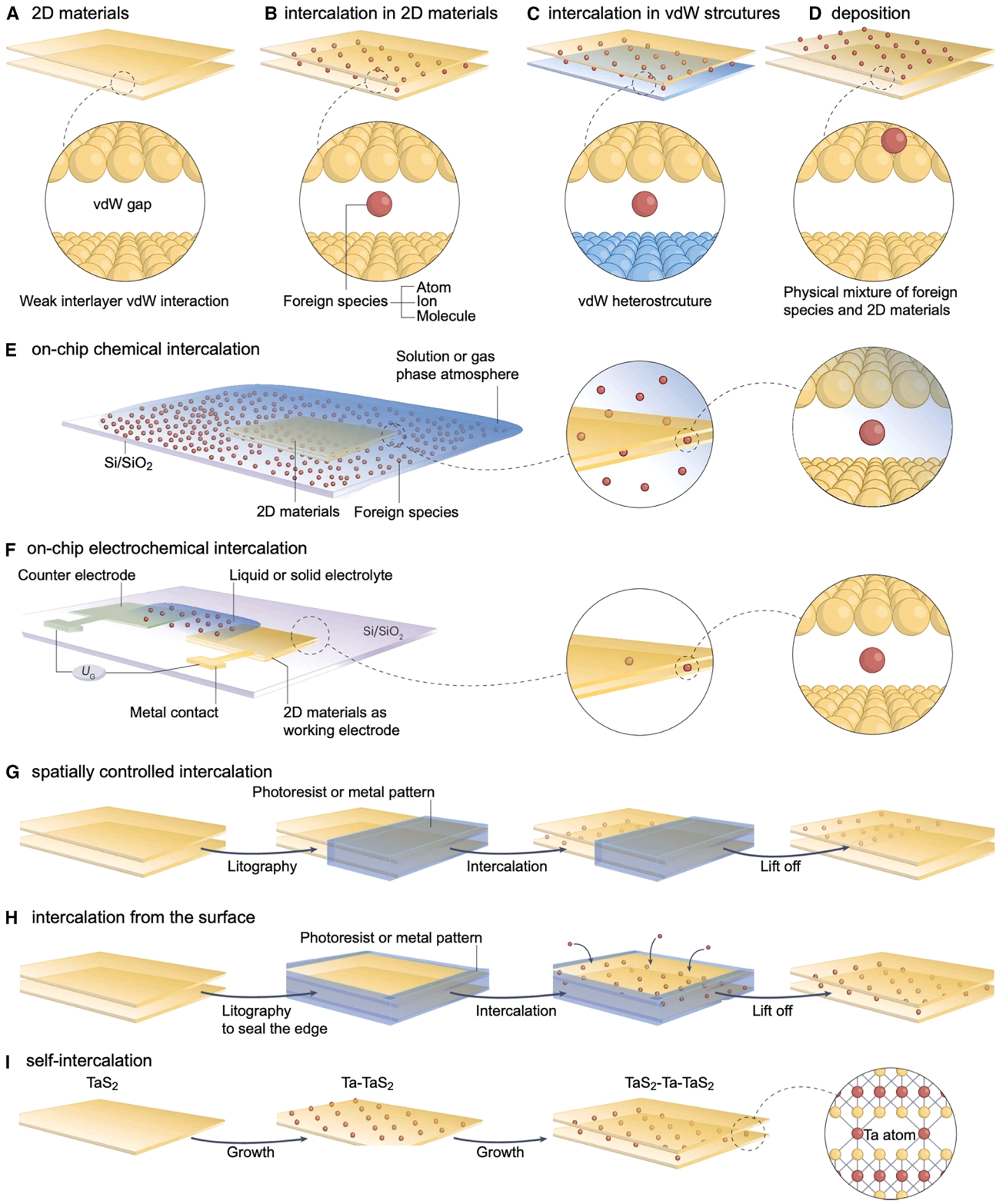

Figure 4. Intercalation in 2D materials

(A) A schematic illustration of 2D materials with weak van der Waals (vdW) interactions between adjacent layers.

(B) Foreign species intercalated between the 2D layers could be atoms, ions, or molecules.

(legend continued on next page)

properties such as chiral-induced spin selectivity or tunable dielectric responses.[58]

To meet these diverse aims, a broad range of intercalation strategies has been developed (Figure 4).[57] Among them are: classical chemical approaches rely on solution-based methods or vapor-phase routes; electrochemical intercalation enables subtle control by coupling the insertion process to an applied potential; approaches where molten salts, alloys, or catalytic intermediates to mediate insertion, broadening the palette of accessible intercalants; spatially selective intercalation, in which masking or edge-sealing defines the pathways of guest insertion. Beyond atomic or ionic guests, organic-molecule intercalation has become an expanding field: bulky molecules such as tetracyanoquinodimethane (TCNQ), crown ethers, or porphyrins have been inserted into layered hosts to generate hybrid superlattices with tailored interactions and emergent properties.

The consequences of intercalation are broad and frequently transformative. The immediate structural effect is an expansion of the interlayer spacing, which weakens vdW coupling and can facilitate exfoliation into few-layer or monolayer crystals. In many cases, intercalation triggers phase transitions, such as the canonical transformation of 2H-MoS_2 into metallic 1T or 1T′ phases upon alkali metal insertion[67–69] or changes in the stacking and electronic structure of graphite upon intercalated Li or Ca layers.[70–73] MXenes, a newer class of layered carbides and nitrides, also display tunable electronic and catalytic properties upon intercalation with alkali ions, organic molecules, or even water.[74,75] Electronic effects are equally striking: intercalants donate or accept charge, shifting the Fermi level, modifying band dispersions, and in some cases generating entirely new metallic states. Such effects underpin the use of intercalated systems in electronic and optoelectronic devices. Magnetic responses can also be tuned, with intercalation either stabilizing or suppressing order depending on the balance between host and guest species. For example, Eu intercalation beneath graphene or *h*-BN on Ni(111) or Co(0001) alters local magnetic proximity effects.[76–79] From an applied perspective, the reversibility of these processes is critical: while some systems exhibit highly reversible intercalation cycles, others suffer from structural degradation, side reactions, or irreversible changes, as reflected extensively in electrochemical studies. Organic molecule intercalation adds further dimensions to these effects: functional molecules can introduce symmetry breaking, dipolar fields, or chiral interactions, giving rise to hybrid properties such as enhanced spin filtering or unusual thermoelectric behavior.[58]

PROPERTIES OF BULK METAL PHOSPHORUS TRICHALCOGENIDES MATERIALS

In recent years, layered vdW materials have attracted enormous attention as platforms for exploring novel physical phenomena and enabling applications in electronics, energy, and catalysis.[80,81] Beyond graphene and transition metal dichalcogenides (TMDs), which have dominated the early landscape of two-dimensional materials, transition metal phosphorus trichalcogenides (TMTs) (MPX_3, where M = transition metal and X = chalcogen) have emerged as a particularly intriguing class. These compounds combine structural flexibility with rich electronic and magnetic phenomena, setting them apart from other vdW systems.[28–34]

Crystallographically, MPX_3 materials adopt either the monoclinic *C*2/*m* (sulphides) or the rhombohedral $R\bar{3}$ (selenides) space groups, with subtle differences in interlayer stacking that influence their interlayer coupling (Figures 6A–6D). Each MPX_3 layer consists of a honeycomb lattice of M^{2+} cations, with every hexagon centered by a P-P dimer. The phosphorus atoms are tetrahedrally coordinated by chalcogen atoms, forming PX_3 pyramids that terminate the layer on both sides. Such an arrangement results in weak interlayer vdW forces and allows facile exfoliation into few-layer or monolayer systems. A unique feature of MPX_3 is the coexistence of three types of bonding – ionic, covalent, and vdW – within the same lattice, which gives rise to a broad spectrum of tunable physical properties. Importantly, unlike TMDs, most MPX_3 compounds exhibit intrinsic magnetic order due to the localized 3*d* electrons of the transition metal cations. Along with that, the interaction between magnetic moments is governed by the competition between direct M-M antiferromagnetic exchange and indirect M-X-M ferromagnetic superexchange. This interplay results in a remarkable diversity of magnetic ground states. For example, $MnPS_3$ adopts a Heisenberg-type Néel AFM ordering with a Néel temperature of ~87 K, $FePS_3$ exhibits Ising-like zigzag AFM order with $T_N \approx 118$ K, $CoPS_3$ shows XXZ stripy AFM order with $T_N \approx 120$ K, and $NiPS_3$ displays XXZ zigzag AFM ordering with $T_N \approx 158$ K.[31,83] Such diversity illustrates the sensitivity of the magnetic ground state to the electronic configuration of the transition metal ion. This magnetism, combined with semiconducting band gaps in the range of 1.2–3.5 eV (e.g., Figure 6F), positions MPX_3 as a multifunctional material at the crossroads of magnetism, optoelectronics, and catalysis. From the electronic structure perspective, MPX_3 are wide-gap semiconductors, with values depending strongly on the specific metal and

(C) Beyond 2D materials, intercalation can also happen in their vdW heterostructures.
(D) Deposition is favored over intercalation when the intercalated compound is less thermodynamically stable than the physical mixture of the foreign species and 2D materials in a given environment.
(E) Chemical intercalation occurs by immersing 2D materials into an intercalant solution or exposing them to vaporized intercalants.
(F) Electrochemical intercalation normally runs on an on-chip electrochemical cell, in which the targeted 2D material is a working electrode and connects with a patterned metal contact. A counter electrode and electrolyte containing the ionic intercalants complete the electrical circuit. U_G, voltage.
(G) Spatially controlled intercalation is achieved by locally wrapping the 2D materials (through photoresists or metal patterns), followed by an intercalation process before the wrap is lifted off(removal of photoresist or metal pattern).
(H) When the edges of 2D materials are fully sealed by photoresists or metal patterns, small atoms or ions may intercalate into the vdW gaps of 2D materials from the top surface.
(I) Self-intercalation is when the intercalation species is a native atom rather than foreign, such as tantalum (Ta) intercalation into 2D tantalum disulfide (TaS_2).
Reproduced with permission.[57] Copyright 2024, Springer Nature Limited.

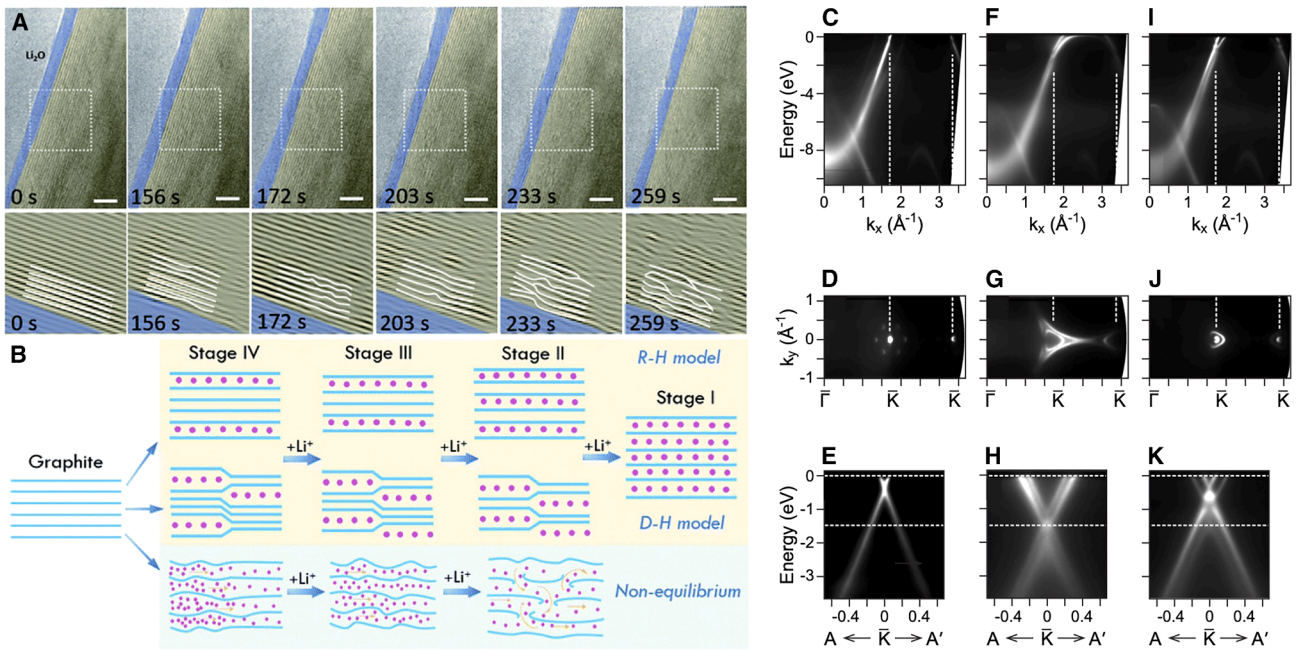

Figure 5. Li-intercalation in graphite

(A and B) Structural evolution during the *in situ* lithiation of graphite: (A) *In situ* HRTEM images and corresponding filtered TEM images showing the d-spacing expansion and interlayer distortion during lithiation. Bottom: inverse fast Fourier transform (IFFT) images. Scale bars of (A) are 5 nm. The Li_2O layer is colored blue, and the graphite layer is colored yellow. (B) Schematic of equilibrium (R–H model and D–H model) and non-equilibrium lithiation processes during the Li-ion insertion into the graphite layers. The blue lines represent the graphite layers and the red balls represent lithium ions. Reproduced with permission.[59] Copyright 2021, The Royal Society of Chemistry.

(C–K) Band dispersion recorded from monolayer graphene samples before [(C–E)] and after [(F–H)] Li deposition, and after heating to 300° C [(I–K)]. The dashed lines are guides to the eye for illustrating the location of the first and second K points or an initial state energy of 0 eV and −1.4 eV. The Fermi energy is located at 0 eV. Reproduced with permission.[60] Copyright 2016, American Physical Society.

chalcogen combination. Here, within the Zaanen-Sawatzky-Allen classification,[84] $MnPX_3$ and $FePX_3$ are described as Mott-Hubbard insulators,[85–89] $NiPS_3$ is a charge-transfer insulator,[89–91] and $CoPS_3$ exhibits mixed character.[92,93] This diversity reflects the fine balance between on-site Coulomb electron repulsion on the 3*d* orbital of the magnetic ion (U_{dd}) and charge-transfer energy between ligand and magnetic ion (Δ), parameters that can be tuned by external perturbations such as strain, chemical doping, or substrate interactions.[31,34]

MPX_3 materials can be engineered using various strategies, including defects' formation, alloying, adsorption, and intercalation.[28,34] Defect engineering, particularly the creation of chalcogen or phosphorus vacancies, often occurs naturally during exfoliation. Such vacancies can reduce the band gap, introduce midgap states, and in some cases induce weak ferromagnetism due to sublattice imbalance.[94] Electron beam irradiation experiments have shown that controlled defect creation can even drive transformations into new crystallographic phases.[95–97] Alloying provides another powerful route: substitution of transition metals tunes anisotropy and exchange interactions, while high-entropy alloys with multiple metals expand the compositional space and promote enhanced ion diffusion in electrochemical applications.[98–101] Adsorption of small molecules, such as H_2O, CO_2, and NO_2, also strongly influences the properties of MPX_3, especially in the presence of vacancies.[102–104] For instance, NO_2 adsorption on $MnPS_3$ leads to strong bonding and modifies magnetic anisotropy, while CO_2 adsorption on $FePS_3$ has been associated with catalytic conversion pathways to methanol and ethanol.[105–107] Perhaps the most versatile modification strategy is intercalation (Figures 6G–6L). Alkali metals and organic cations can be inserted into the vdW gaps, either through redox-active processes that involve changes in the oxidation state of the host lattice or through non-redox ion-exchange processes. These modifications can induce ferrimagnetism, enhance conductivity, or tailor electrochemical activity, often in a reversible manner[82,108–111] (Figures 6I–6L).

The combination of tunable semiconducting behavior and the possibility of intercalation in the space between vdW layers naturally suggests opportunities in energy-related applications. MPX_3 materials have been investigated as hosts for Li-, Na-, and Mg-ion batteries, where their layered structure supports ion intercalation. Depending on the MPX_3 material, both redox and non-redox mechanisms are possible, which have important implications for cycling stability and capacity. The layered nature of MPX_3 also makes them attractive candidate for hydrogen storage, where both physisorption and chemisorption pathways are accessible, especially in vacancy-rich systems. Furthermore, their band-gap edges' positions relative to water redox potentials make them promising for HERs and OERs in water splitting (Figure 7).[112] The catalytic activity of

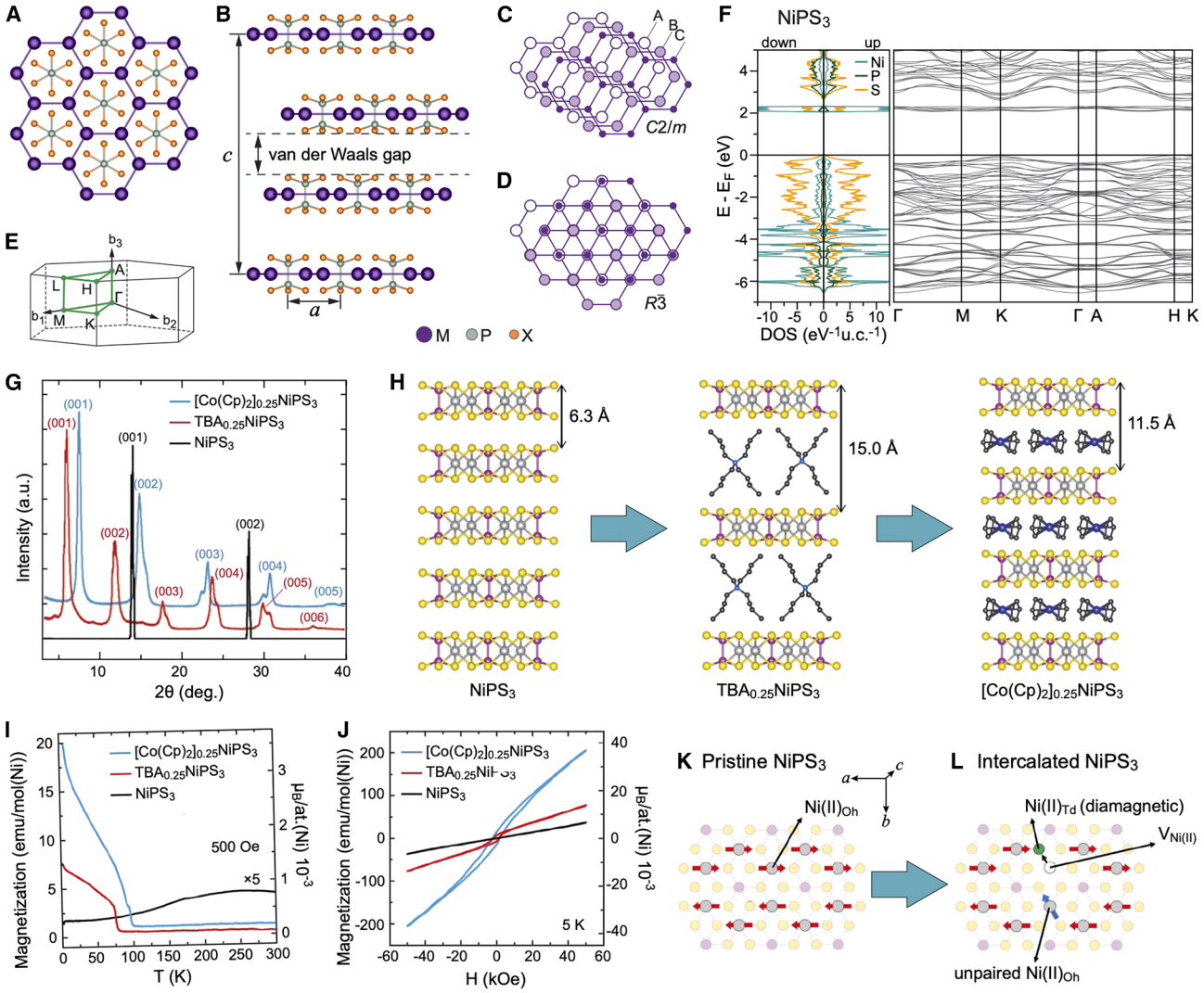

Figure 6. Properties of bulk MPX_3 materials

(A–D) Crystallographic structure of bulk MPX_3 crystals: (A) top view of a single MPX_3 layer; (B) crystal structure of 3D MPX_3; (C and D) different stackings in bulk MPX_3 corresponding to *C2/m* and $R\bar{3}$ space groups, respectively. For simplicity, only M-ions are shown. Atoms of different layers are shown with spheres of different sizes and styles; (E) Brillouin zone for 3D MPX_3 in the hexagonal representation.

(F) Calculated atom projected DOS and band structures for bulk $NiPS_3$. Reproduced with permission.[31] Copyright 2023, IOP Publishing.

(G–L) Experiments on the intercalation of organic ions in bulk $NiPS_3$: (G) XRD patterns of bulk $TBA_{0.25}NiPS_3$ and $[Co(Cp)_2]_{0.25}NiPS_3$ in comparison with those of bulk $NiPS_3$; (H) scheme of the intercalation and ion exchange when going from bulk $NiPS_3$ through $TBA_{0.25}$ $NiPS_3$ to $[Co(Cp)_2]_{0.25}NiPS_3$. The respective interlayer distances are marked in the figure; (I) field-cooled molar magnetization versus temperature for bulk $NiPS_3$, $TBA_{0.25}$ $NiPS_3$, and $[Co(Cp)_2]_{0.25}NiPS_3$ crystals. The applied field (500 Oe) is oriented parallel to the *ab* plane of the crystal; (J) hysteresis loops at 5 K of bulk pristine $NiPS_3$, $TBA_{0.25}NiPS_3$, and $[Co(Cp)_2]_{0.25}NiPS_3$ crystals; (K and L) Scheme of the structural change in the $NiPS_3$ layer accompanying the reduction of the Ni atoms. Reproduced with permission.[82] Copyright 2022, The Royal Society of Chemistry.

MPX_3 can be enhanced through defect engineering and intercalation, which modify the adsorption energies of key reaction intermediates.

Beyond these conventional applications, MPX_3 is also a promising platform for confined catalysis. Their intrinsic vdW gaps, ability to host intercalated species, and compatibility with 2D heterostructures create natural reaction chambers at the nanoscale. These confined environments can stabilize reaction intermediates and alter reaction pathways, similar to concepts realized in TMDs and porous frameworks. The multifunctionality of MPX_3 – combining semiconducting behavior, magnetism, and catalytic activity within a single family – opens opportunities for designing devices that integrate spintronics, energy storage, and catalysis. Remaining challenges include improving conductivity, scaling up synthesis, and ensuring stability under operating conditions. Addressing these issues will be critical for unlocking the full potential of MPX_3 in confined catalysis and energy technologies.

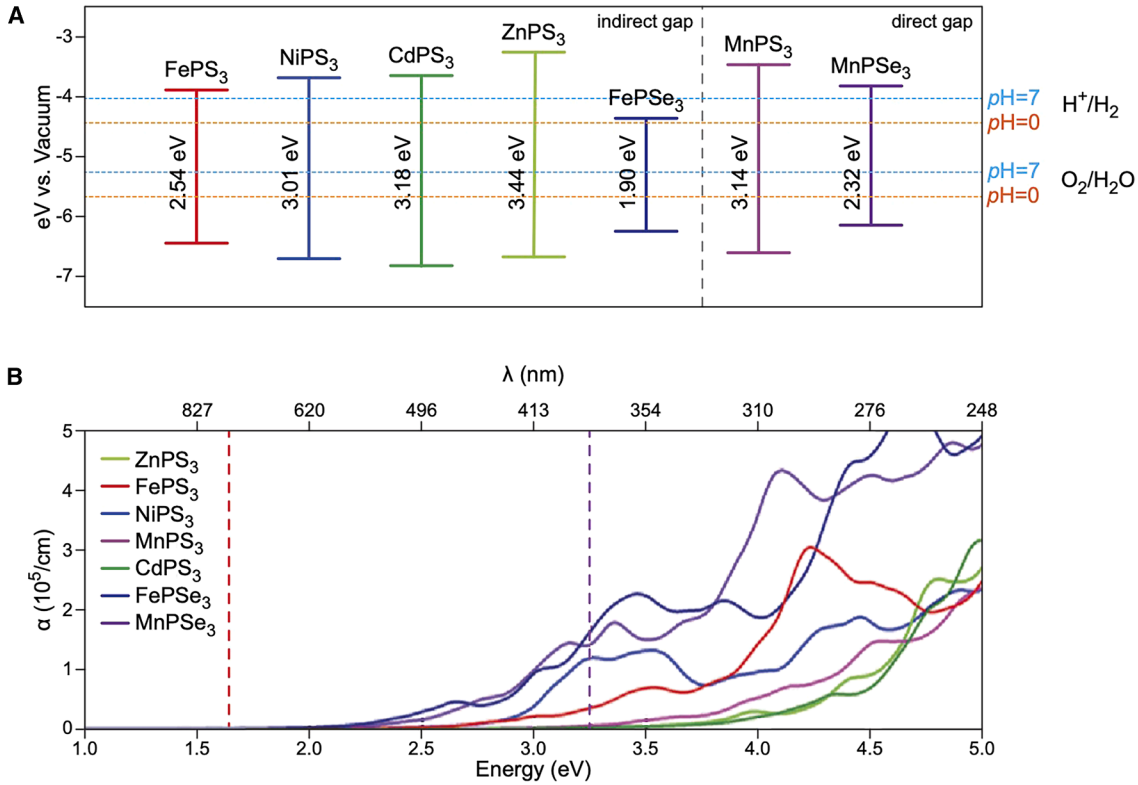

Figure 7. Properties of MPX_3 for water splitting applications

(A) The location of valence band maximum and conduction band minimum calculated with the HSE06 functional of MPS_3 and $MPSe_3$ monolayers. The redox potentials of water splitting at pH = 0 (orange dashed lines) and pH = 7 (cyan dashed lines) are shown for comparison.

(B) Optical absorption coefficient α for MPS_3 (M = Fe, Mn, Ni, Cd, Zn) and $MPSe_3$ (M = Fe, Mn). The area between the red and the purple lines represents the visible range. Reproduced with permission.[112] Copyright 2016, John Wiley and Sons.

METAL PHOSPHORUS TRICHALCOGENIDES MATERIALS FOR CONFINED CATALYSIS

Layered MPX_3 materials provide a particularly versatile platform for spatial or/and electronic confinement due to their vdW stacked lattices combining accessible interlayer galleries with a flexible electronic structure that tolerates vacancies, dopants, intercalants, and heterostructure formation.[8,33,34,113] Confinement in MPX_3 is inherently multi-modal: it can manifest through interlayer chemical confinement via cation or molecular intercalation, atomic-scale electronic pockets created by vacancies and heteroatom substitution, geometric confinement at interfaces with conductive or porous supports, and electrostatic confinement driven by built-in polarization fields at heterojunctions. Each of these modes reshapes the potential energy surface encountered by intermediates and charge carriers, thereby lowering activation barriers, tuning binding geometries, and accelerating charge transfer in catalytic cycles.

Interlayer confinement

The vdW interlayer space in MPX_3 provides a natural template for confined catalysis. Unlike rigid frameworks, these interlayer spaces are dynamic and tunable, able to host ions or molecules that modify both structure and reactivity.[82,108,110,111,114] For example, *operando* spectroscopic studies of $NiPS_3$ intercalated with different cations have revealed distinct confinement regimes.[42] The overall experimental approach employed by the authors involves synthesizing high-quality $NiPS_3$ and conducting *operando* XRD and XAS to monitor structural and electronic changes during the intercalation of Li, Na, and $EMIM^+$ cations (Figure 8). This approach allows for the real-time observation of the intercalation processes and their effects on the material's properties. It was concluded that the intercalation of Li and Na into $NiPS_3$ involves distinct charge compensation mechanisms, with Li primarily affecting the $(P_2S_6)^{4-}$ unit and Na leading to Ni reduction. The intercalation of $EMIM^+$ cations, while resulting in structural expansion, does not alter the electronic states of the host material, indicating a unique interaction mechanism. The authors acknowledge potential limitations in their study, such as the need for further exploration of the long-term stability of the intercalated phases and the effects of different intercalation conditions. It is suggested that future work should focus on understanding the implications of these findings for the development of hybrid systems based on 2D materials for applications in energy storage and catalysis.

These findings demonstrate that interlayer confinement in MPX_3 is not a single effect, but a tunable continuum: intercalants can introduce redox activity, steric sieving, or purely geometric expansion depending on their size and charge. For catalytic

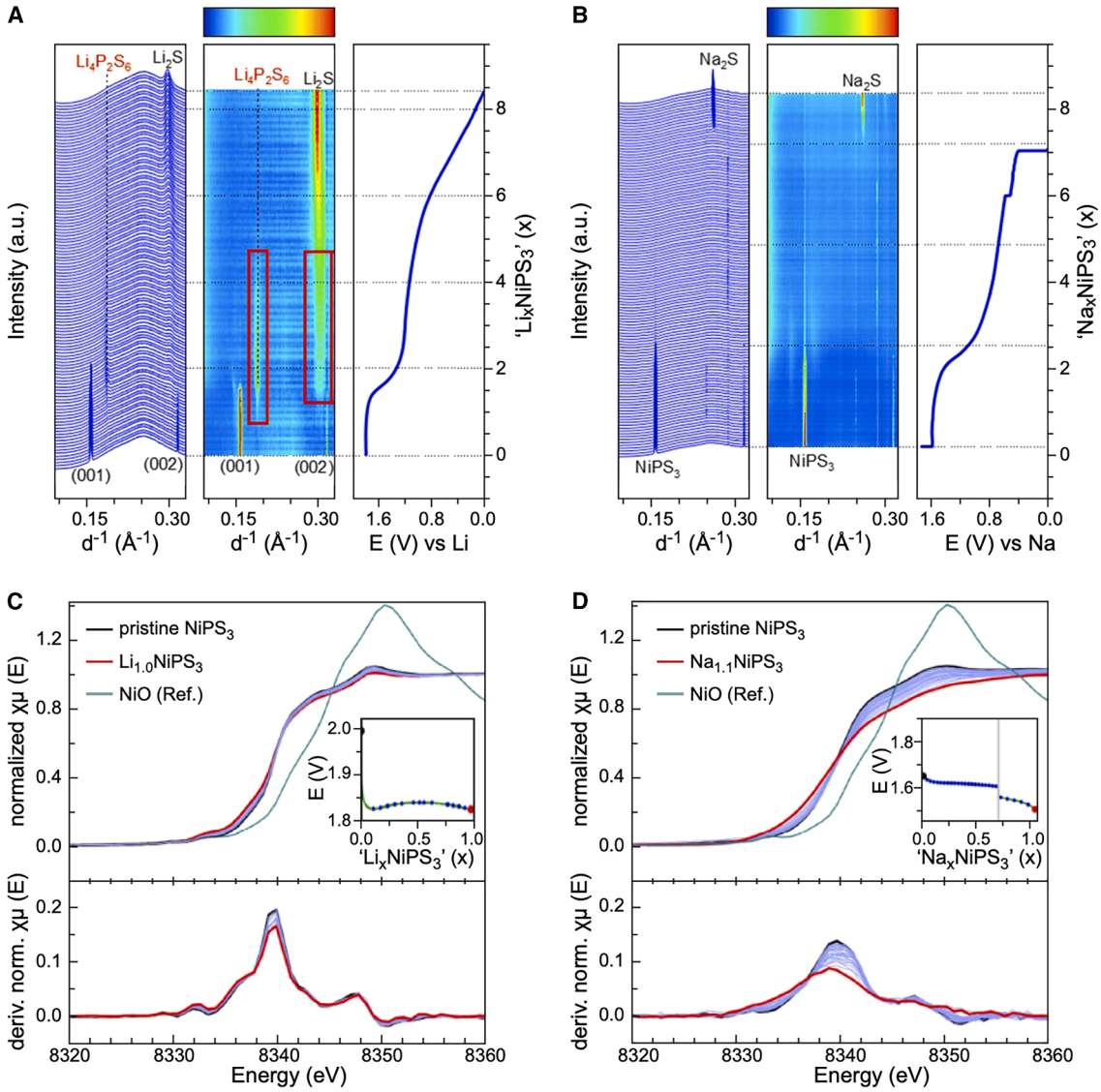

Figure 8. *Operando* spectroscopy of $NiPS_3$ intercalation

(A and B) Waterfall plot, contour plot, and potential profile from operando XRD: (A) Li_xNiPS_3, with a current density of 71 mA/g; red boxes highlight the intermediate phase, and (B) Na_xNiPS_3 with a current density of 61 mA/g.

(C and D) Operando XAS spectra of alkali ion intercalation into $NiPS_3$: (C) Ni *K*-edge and $d\mu(e)/dE$ plots of Li_xNiPS_3 ($0 \leqslant x \leqslant 1$), (D) Ni *K*-edge and $d\mu(e)/dE$ plots of Na_xNiPS_3 ($0 \leqslant x \leqslant 1.1$). Insets show the corresponding potential profiles and the specific points of measurement. Reproduced with permission.[42] Copyright 2024, The Royal Society of Chemistry.

reactions, such as OER or HER, this means that intercalants can modulate local redox potentials, alter solvent structuring, or control intermediate binding through steric effects. The interlayer space thus acts as a confined catalytic chamber, where both electronic and geometric factors can be adjusted *in situ*. This tunability distinguishes MPX_3 from many other layered materials and underscores the value of intercalation chemistry as a strategy for designing catalytic confinement.

Defect-driven confinement

Vacancies and substitutional dopants provide one of the most direct strategies to engineer confined catalytic environments in MPX_3 materials. In pristine MPX_3 lattices, basal planes often exhibit limited activity due to the absence of undercoordinated atoms or favorable adsorption geometries. For example, in ref. 113, the authors argued, using density functional theory (DFT) calculations, that pristine $FePS_3$ has a high Gibbs free energy change for the rate-determining step of the OER, which limits its performance. It is shown that by introducing vacancies, the coordination environment of nearby metal centers is altered, local symmetry is broken, and electronic density is redistributed. These effects generate nano-pockets, where the electronic structure differs markedly from that of the host lattice. In $FePS_3$, laser ablation in liquids has been shown to generate

high densities of phosphorus and sulfur vacancies, while simultaneously incorporating Co into the lattice (Figures 9A and 9B).[115] Spectroscopic and structural analysis revealed mixed-valence Fe/Co centers and enhanced disorder, consistent with the formation of electronically perturbed domains. These confined regions act as localized reaction centers, stabilizing oxygenated intermediates during OER and lowering the free-energy barriers associated with the rate-determining step. DFT calculations support this picture, predicting significant reductions in the Gibbs free energy change for adsorbate formation at vacancy-rich, Co-doped sites compared with pristine $FePS_3$ (Figures 9C and 9D).[115]

The catalytic improvements associated with vacancies extend beyond increased surface area: they reflect the creation of confined electronic microenvironments that tailor intermediate adsorption. In $NiPS_3$ nanosheets, for example, engineering dual Ni and S vacancies has been shown to strongly modulate the electronic structure, increase conductivity, and optimize hydrogen adsorption energies. These dual vacancies act cooperatively, lowering reaction overpotentials for both HER and OER and stabilizing reactive intermediates under electrochemical operation.[117]

Interface-mediated confinement

Another central mechanism of confinement arises when MPX_3 is coupled to conductive scaffolds or porous hosts, producing interfaces where geometric restriction and electronic coupling work in tandem. $NiPS_3$ nanoparticles immobilized on defective graphene (DG) exemplify this principle.[118] The overall experimental approach used in this work involved synthesizing the $NiPS_3$@DG nanocomposite through a one-step sulphur-phosphidation process of a nickel precursor, followed by a series of characterizations to assess its morphology, structure, and electrocatalytic properties. The authors report that the nanoparticles were successfully anchored onto the graphene surface, which was confirmed through SEM and TEM imaging. The morphology showed that the nanoparticles were well-dispersed, minimizing aggregation, which is crucial for maintaining high catalytic activity. It was found that graphene's topological defects act as anchor points, confining $NiPS_3$ nanoparticles to sub-nanometer domains and preventing aggregation. At the same time, the intimate contact between $NiPS_3$ and the highly conductive carbon lattice ensures that electron transport is confined to ultrashort pathways. This dual effect – physical immobilization and electronic junction confinement – dramatically enhances catalytic turnover. In the following experiments, the $NiPS_3$@DG nanocomposite demonstrated exceptional electrocatalytic performance, exhibiting low overpotentials of 73, 97, and 99 mV at 10 mA cm^{-2} in acidic, neutral, and alkaline conditions, respectively. This study reveals that the $NiPS_3$@DG hybrid can compete with or even surpass commercial Pt/C catalysts, providing insights into the potential for cost-effective, pH-universal electrocatalysts.

Similar effects are achieved with porous nitrogen-doped carbon frameworks hosting $FePSe_3$ nanoparticles (Figures 9E–9N).[116] In this architecture, confinement emerges not only from geometric encapsulation, but also from chemical interactions: nitrogen dopants in the carbon lattice alter local work functions and create proton-attractive sites. Meanwhile, the porous matrix enforces the exposure of edge-rich nanoparticle facets and accelerates mass transport through interconnected channels. As a result, active sites are stabilized against aggregation and corrosion, while simultaneously benefiting from altered electronic surroundings. This demonstrates how confinement at interfaces extends beyond stabilization – it creates hybrid environments where structural restriction, charge redistribution, and facilitated transport converge to maximize catalytic performance.

The importance of interfacial confinement is further underscored by vertical heterostructures that combine crystalline MPX_3 layers with amorphous phases or other functional materials. In these constructs, confined regions form at the interfaces, where lattice mismatch or disordered bonding modifies local coordination. Such confined interfacial environments often exhibit enhanced carrier densities, shorter diffusion lengths, and optimized adsorption geometries, pointing again to confinement as a mechanism that operates at the boundary between structure and electronic function.

Electrostatic confinement

Beyond geometric and chemical strategies, confinement in MPX_3 can also be engineered in the purely electronic domain. Amorphous-crystalline heterostructures between CoFeB and $NiPS_3$ illustrate this concept.[119] As shown in the DFT calculations, at the vertical interface, built-in polarization fields emerge due to charge redistribution between the amorphous and crystalline components. These fields confine electron flow and polarize adsorbed species, producing locally enhanced carrier densities. Electrochemical measurements demonstrate that this electrostatic confinement enables ampere-level current densities at modest overpotentials during OER, far exceeding the performance of pristine MPX_3 or CoFeB alone. Importantly, this form of confinement does not require physical pores; instead, it relies on the spatial confinement of electronic fields and carrier distributions, showing that confinement can be realized even without structural modification. Electrostatic confinement may represent a particularly powerful design route because it can be tuned through interface engineering without introducing instability associated with vacancies or intercalants. By carefully controlling the degree of amorphous-crystalline mismatch, one can shape internal electric fields that accelerate charge transfer and stabilize high-energy intermediates. This highlights the importance of heterostructure design as a frontier in confined catalysis with MPX_3.

From the presented analysis across these modes of confinement, a consistent mechanistic picture emerges. Confinement in MPX_3 enhances catalysis by tuning adsorption energies, lowering activation barriers, and stabilizing high-energy active sites against deactivation. Each strategy demonstrates that confinement is not merely a geometric restriction, but a means to engineer the electronic, electrostatic, and transport environment of catalytic centers. Nevertheless, significant challenges remain before confinement in MPX_3 can be transformed into a predictive design principle. First, quantitative correlations between structural motifs (vacancy density, dopant distribution, interlayer spacing) and catalytic free-energy surfaces remain

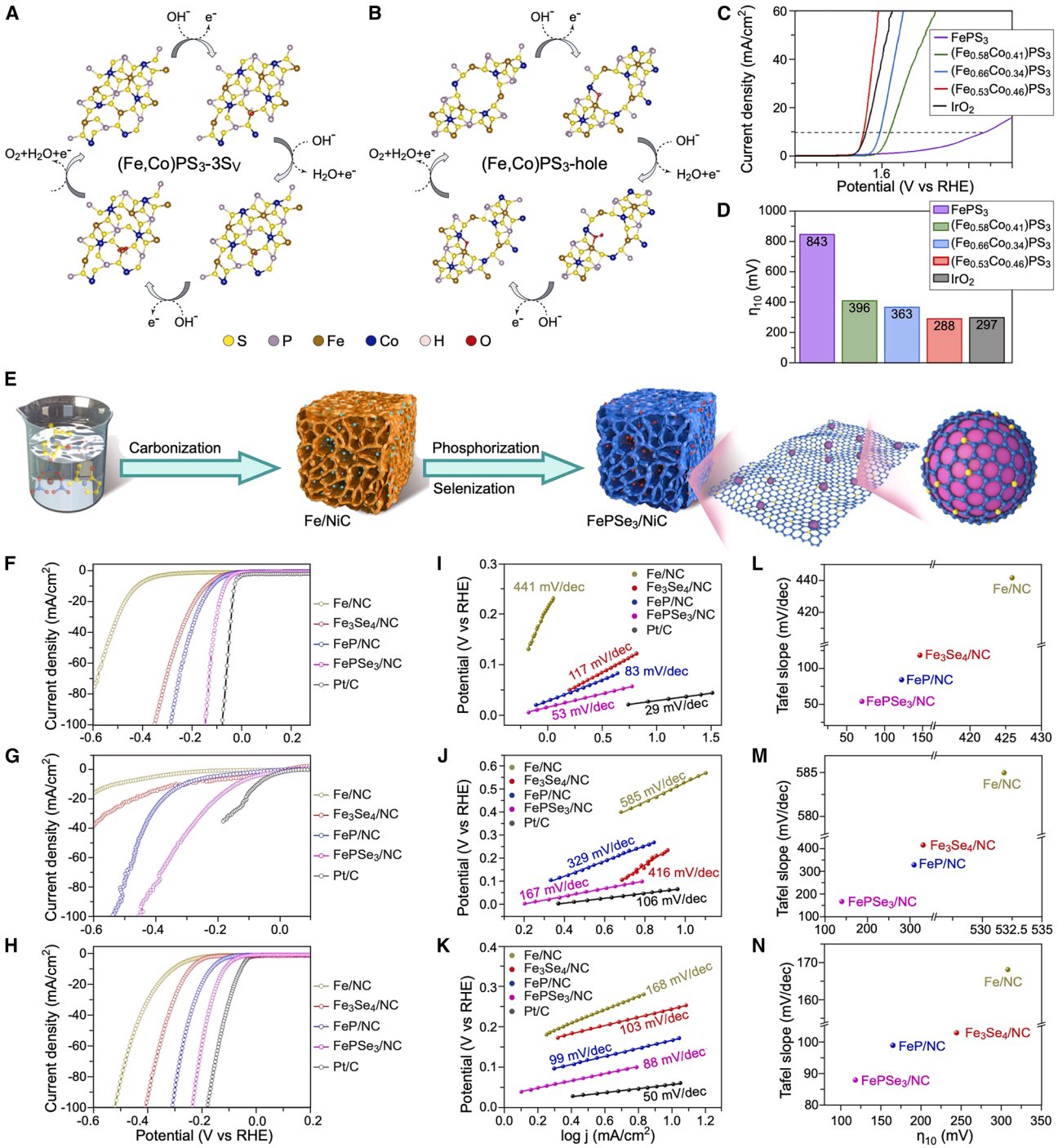

Figure 9. Example of defect- and interface-driven confinement using $FePS_3$

(A and B) The DFT models of the OER process of (Fe,Co)PS_3-3S_v with Fe as active sites (A) and (Fe,Co)PS_3-hole with Fe-Co bridge as active sites(B).

(C and D) Electrocatalytic OER performance of (Fe,Co)PS_3: (C) LSV curves in 1 m KOH electrolyte at a scan rate of 5 mV/s. (D) Overpotentials of $FePS_3$, (Fe,Co)PS_3 and IrO_2 at 10 mA/cm^2. Reproduced with permission.[115] Copyright 2025, John Wiley and Sons.

(E) Schematic illustration of the formation process of $FePSe_3$/NC.

(F–N) Electrochemical HER measurements. LSV curves of 20% wt Pt/C, Fe/NC, Fe_3Se_4/NC, FeP/NC, and $FePSe_3$/NC in 0.5 M H_2SO_4 (F), 1 M PBS (G), and 1 M KOH (H), respectively. The corresponding Tafel plots of 20% wt Pt/C, Fe/NC, Fe_3Se_4/NC, FeP/NC, and $FePSe_3$/NC in 0.5 M H_2SO_4 (I), 1 M PBS (J), and 1 M KOH (K), respectively. The comparison of overpotentials at j = 10 mA/cm^2 and Tafel slopes in 0.5 M H_2SO_4 (L), 1 M PBS (M), and 1 M KOH (N), respectively. Reproduced with permission.[116] Copyright 2018, Elsevier Ltd.

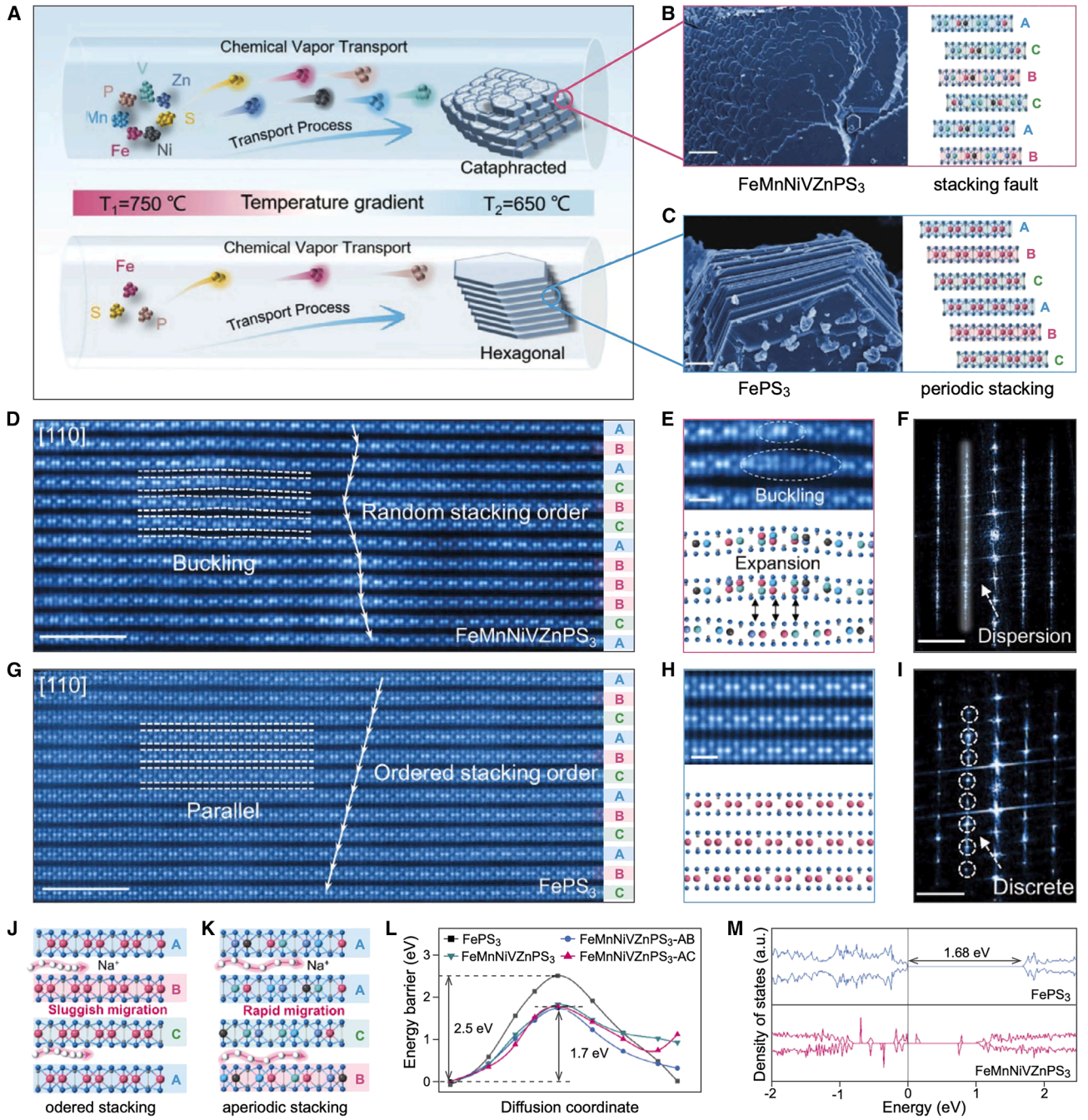

Figure 10. Application of high-entropy MPX_3 compounds in sodium-ion systems (batteries)

(A) The schematic diagram depicts the controlled growth of high-entropy $FeMnNiVZnPS_3$ and $FePS_3$ by CVT.

(B and C) SEM images of $FeMnNiVZnPS_3$ (B) and $FePS_3$ (C) showing the structural morphology. Corresponding atomic models were depicted on the right panels.

(D) The cross-section STEM-ADF image of $FeMnNiVZnPS_3$ viewed along the [110] zone axis. Different stacking sequences, i.e., *A*, *B*, and *C*, highlighted by blue, red, and green false colors, respectively, were depicted on the right.

(E) Zoom-in STEM-ADF image shows the buckling region and the corresponding atomic model is shown on the bottom.

(F) The FFT of an extended region from (d).

(G) The cross-section STEM-ADF image of $FePS_3$ viewed along the [110] zone axis.

(H) Zoom-in STEM-ADF image of $FePS_3$ showing a flat nature, and the corresponding atomic model is depicted later in discussion.

(legend continued on next page)

limited. *Operando* and *in situ* probes capable of tracking confinement under working conditions – such as spectroscopies with spatial resolution down to individual vacancies – are urgently needed. Second, stability under realistic conditions is not yet established: vacancies may heal, intercalants may migrate, and heterostructures may reconstruct during extended operation, erasing confinement effects. Third, synthetic methods must evolve to deliver confinement motifs in scalable and reproducible ways; current approaches, such as laser ablation or solution-based hybridization of MPX_3-based catalyst components, remain primarily at the proof-of-concept stage. Thus, future opportunities lie in integrating multiple confinement strategies into single architectures – for example, coupling interlayer expansion with interface stabilization, or combining vacancy engineering with electrostatic heterojunctions. Computational screening can accelerate this process by predicting how different confinement modes modify adsorption landscapes, guiding targeted synthesis. Beyond catalysis, the unique capacity of MPX_3 to couple spin, charge, and lattice degrees of freedom suggests that confinement strategies could also be extended to magnetically modulated electrocatalysis, a direction scarcely explored.

METAL PHOSPHORUS TRICHALCOGENIDES MATERIALS FOR BATTERY APPLICATIONS AND HYDROGEN STORAGE

The capacity of layered MPX_3 compounds to function across multiple energy-storage and hydrogen-related technologies is rooted in their vdW layered geometry, adaptable interlayer spacing, and electrochemically active transition-metal centers. These structural features allow MPX_3 to accommodate both intercalation-type and conversion-type reactions. The same materials' family can be engineered to behave either as an ion-storage host or as an electrocatalyst, depending on composition, defect density, and heterostructuring with conductive phases. This multifunctionality has been emphasized in recent reviews, which highlight MPX_3 as a versatile platform for both batteries and hydrogen technologies.[33,34,120–123]

Metal phosphorus trichalcogenides for battery applications

In lithium-ion batteries (LIBs), MPX_3 anodes frequently demonstrate a combination of intercalation (Li_xMPX_3) at low lithiation and conversion to Li_2 X/Li_3 P products plus reduced metal at deeper discharge, a duality that explains both the high specific capacities reported and the necessity for structural engineering to preserve cycle life (overall deep conversion is commonly written as: $MPX_3 + 9Li^+ + 9e^- \rightarrow 3Li_2X + Li_3P + M$.[123–125] Experimental reports demonstrate practical device performance when MPX_3 are nanoscaled or combined with other components: exfoliated $MnPS_3$ nanosheets maintain several hundred mA·h·g^{-1} over extended cycling and show structural resilience in *in situ* TEM studies[126]; $NiCoPS_3$ embedded in N-doped graphitic carbon ($NiCoPS_3$/NC) exhibits capacities near 780–830 mA h g^{-1} with thousands of cycles at moderate to high current densities.[122] Recent defect-engineering studies confirm that deliberate sulfur or phosphorus vacancy creation reduces lithiation barriers and increases conductivity, further boosting rate capability and retention.[115]

Sodium-ion systems (batteries) (SIBs) take advantage of wide interlayer spacing: MPX_3 compounds such as $FePS_3$, $NiPS_3$, and their derivatives achieve high reversible Na storage by combining intercalation with conversion pathways. When coupled with conductive scaffolds (graphene, MXene, N-doped carbons), they deliver both high capacity and competitive full-cell energy densities. $FePS_3$@MXene anodes paired with $Na_3V_2(PO_4)_3$ cathodes produced full-cell energy densities reported near 424 Wh·kg^{-1} (ref.[127]). Propylamine-intercalated $NiPS_3$ nanosheets deliver exceptionally high capacities (1090 mA h g^{-1} at low rates and 536 mA h g^{-1} at high rates), demonstrating how interlayer chemistry substantially alters sodium kinetics.[128] A later study reported that intercalation and defect engineering of layered $MnPS_3$ yield enhanced capacity and stability, confirming the importance of synergistic structural/electronic tuning.[129] Here, high-entropy MPX_3 compounds ($FeMnNiVZnPS_3$) were recently proposed to accelerate Na^+ diffusion via creating the so-called strain soliton boundaries, which serve as sites for localized electric field enhancement, achieving faster kinetics and improved retention (Figure 10).[100]

Potassium-ion batteries (PIBs) confront still larger ion radii, but MPX_3 nanosheets and heterostructures provide workable hosts. Few-layer $FePSe_3$-CNT and $FePSe_3$-graphite hybrids have been shown as stable PIB anodes with capacities between ~200–540 mA h g^{-1} depending on architecture and loading, and they retain good cycling performance when nanoscale morphology and conductive scaffolds stabilize volume changes.[123,130,131] The main enabling strategies here are (i) morphological thinning to shorten K^+ diffusion lengths, (ii) formation of 2D/1D or 2D/2D heterostructures to prevent restacking and buffer expansion, and (iii) electronic percolation networks to offset intrinsic semiconducting behavior. For example, $FePSe_3$-$FeSe_2$ heterojunctions in a carbon matrix showed ≈352 mA h g^{-1} at 0.1 A g^{-1} after 100 cycles and ≈224 mA h g^{-1} at 1.0 A g^{-1} after 3700 cycles, illustrating stable long-term cycling.[130,131]

Multivalent carriers (Mg^{2+} and other divalent ions) present stronger coulomb interactions and sluggish solid-state mobility, yet MPX_3 demonstrates measurable reversible Mg intercalation under carefully selected electrolytes. Work with all-phenyl complex (APC) electrolytes demonstrated reversible Mg insertion into $FePS_3$ with combined faradaic and pseudocapacitive storage; $FePS_3$ retained appreciable capacity (~102 mA h g^{-1} in early reports) and structural integrity, whereas $FePSe_3$ was less accommodating (Figure 11).[125,132] These results indicate that careful tuning of electrolyte chemistry and host vacancies

(I) The FFT of an extended region from (g).
(J and K) The schematics showing the Na^+ ion diffusion path in (J) ordered $FePS_3$ and (K) aperiodic stacked $FeMnNiVZnPS_3$.
(L) The calculated energy barrier for Na^+ diffusion in $FePS_3$ (black curve), and *AA*-(green), *AB*-(blue), and *AC*-(pink) stacked $FeMnNiVZnPS_3$.
(M) The calculated total DOS of $FePS_3$ (blue curve) and $FeMnNiVZnPS_3$ (pink curve). Reproduced with permission.[100] Copyright 2024, John Wiley and Sons.

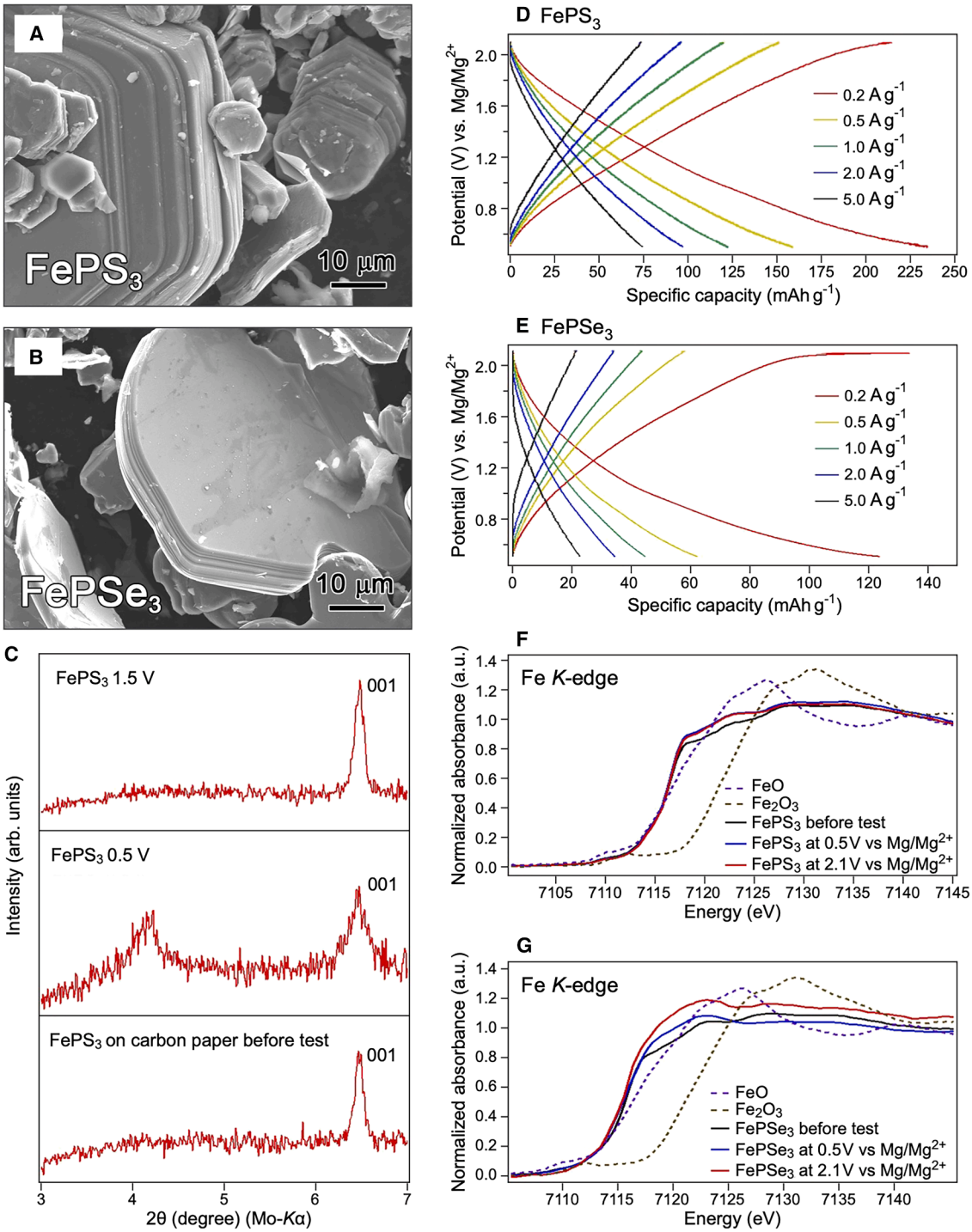

Figure 11. Application of MPX_3 for multivalent (Mg^{2+}) ions storage

(A and B) SEM images of (A) $FePS_3$ and (B) $FePSe_3$.

(C) *Ex situ* XRD patterns of $FePS_3$ on carbon paper. The $FePS_3$ electrode was cathodically swept from OCP to 0.5 V vs. Mg/Mg^{2+} and held for 3 h, and then anodically swept to 1.5 V vs. Mg/Mg^{2+} and again held for 3 h in 0.4 M APC, at a scan rate of 0.1 mV/s. Discharge/charge curves for (D) $FePS_3$ and (E) $FePSe_3$ measured in 0.4 M APC. Normalized Fe *K*-edge XANES spectra for (F) $FePS_3$ and (G) $FePSe_3$ electrodes before electrochemical testing, after discharge at 0.5 V for 3 h, and subsequent charge at 2.1 V for 3 h in 0.4 M APC. Normalized Fe *K*-edge XANES spectra of FeO and Fe_2O_3 are shown as a reference. Reproduced with permission.[125] Copyright 2021, Elsevier B. V.

can make MPX_3 viable for multivalent energy storage, though electrolyte-electrode compatibility remains the main bottleneck. Recent computational screening suggests mixed S/Se chalcogen substitution and vacancy modulation can lower Mg^{2+} migration barriers by 20–30%, pointing to future rational design.[33]

Zinc-air batteries (ZABs) shift emphasis away from bulk ion storage to electrocatalysis: the ORR/OER kinetics at the air cathode control energy efficiency, and MPX_3 nanosheets (especially surface-modified or anion-substituted variants) have emerged as competent bifunctional catalysts. Oxygen-doped $FePSe_3$ produced by plasma treatment and Se-tuned $NiPS_3$ show high bifunctional activity, long cycle life, and mechanical flexibility in solid-state ZAB prototypes, sometimes rivalling noble-metal benchmarks.[124,131] The catalytic improvement is commonly rationalized by bandgap narrowing, optimized adsorption energetics, and crystalline-amorphous surface reconstructions that increase active-site density.[124,131,133]

The emergence of all-solid-state batteries (ASSBs) reinforces the attractiveness of MPX_3 as electrode materials with intrinsic mixed conduction. $FePS_3$ and $NiPS_3$ electrodes have been successfully integrated with sulfide solid electrolytes, showing reversible Li_x insertion/extraction and discharge capacities exceeding 300 mA h g^{-1} without the need for conductive additives in some configurations.[130,132] The interlayer accommodation and mixed transport in certain MPX_3 compositions reduce the complexity of composite electrode formations, but continued attention is required for electrode-electrolyte interfacial stability and scalable electrode processing. Recent work suggests that thin oxide or phosphide coatings can suppress parasitic reactions at MPX_3/sulfide interfaces, improving cycle stability in ASSBs.[134]

Metal phosphorus trichalcogenides *for hydrogen storage*

Hydrogen storage and hydrogen evolution chemistry are areas where MPX_3 can contribute both as sorbents and as electrocatalysts. Early experimental studies demonstrated that $FePS_3$ and related MPS_3 compounds can uptake hydrogen in their vdW gaps (adsorption isotherms were reported decades ago for $FePS_3$), and DFT work has since assessed binding energetics and optimal functionalization routes.[121,135] Computational studies show that hydrogen adsorption on $MnPS_3$ and other MPX_3 surfaces is energetically favorable under certain defect/doping conditions and that vacancy creation enhances H-binding by adjusting local charge distribution.[102–104] More recent experimental and computational efforts target reversible hydrogen storage by combining moderate binding enthalpies (to allow desorption under mild conditions) with high areal density: vacancy engineering, heteroatom substitution (e.g., partial O incorporation), and metal substitution have all been shown to move the adsorption enthalpy toward the desirable window for practical uptake/release.[136–138]

Regarding catalysis for HER and coupled hydrogen production/storage cycles, layered MPX_3 materials show significant promise. Experimental reports introduced $FePS_3$ as an inexpensive, wide-pH-range electrocatalyst for HER, and subsequent studies have improved performance by edge activation, partial oxidation, doping (Co-doping into $FePS_3$), and heterostructuring with classical catalysts (e.g., MoS_2) to synergistically increase active site density and accelerate kinetics.[135,139,140] DFT studies have clarified that basal planes are often inert but that edges, vacancies, and single-atom metal decoration convert basal sites into active centers with near-optimum hydrogen adsorption free energies, a key descriptor for HER performance. This combination of computational and experimental evidence supports a roadmap in which MPX_3 is engineered as a bifunctional hydrogen catalyst and as a moderate-enthalpy storage host, enabling catalytic adsorption plus release schemes for chemical hydrogen storage.

Because hydrogen storage requires both reversible adsorption and practical gravimetric/volumetric metrics, MPX_3 is unlikely to beat MOFs or high-surface-area physisorbents in raw H_2 uptake at cryogenic conditions. Their advantage lies in integrated device concepts: MPX_3-based composites that combine adsorption, catalytic activation, and facile release (HER) in the same material may enable compact, safe, and on-demand hydrogen systems for niche applications (e.g., combined hydrogen storage plus electrochemical conversion modules). Computational strategies (high-throughput DFT screening, strain/doping maps) are being used to identify MPX_3 compositions with adsorption free energies near the thermo-neutral window ($\Delta G_H \approx 0$ eV) and reasonable binding energies for reversible storage at ambient or mild conditions.[141,142]

Across all chemistries, the recurring engineering solutions are clear: exfoliation/nanoscaling to shorten ion diffusion distances and exposing edge sites; vacancy/defect engineering and heteroatom doping to tune adsorption energies and electronic structure; and heterostructuring with conductive scaffolds (graphene, CNTs, MXenes, N-doped carbons) to supply electron percolation and mechanically buffer volumetric changes. These approaches have already yielded functioning device prototypes: $FePS_3$@MXene anodes in sodium full cells, $NiCoPS_3$@N-carbon anodes for high-rate LIBs, $FePSe_3$/CNT hybrids for PIBs, and O-doped $FePSe_3$ cathodes for flexible ZABs. The path to practical deployment, therefore, appears technical rather than conceptual: scalable, defect-controlled synthesis, electrode-electrolyte compatibility studies (especially for multivalent electrolytes), realistic full-cell tests (loadings, areal capacities, lean electrolyte), and lifetime/thermal stability metrics must be prioritized.

CONCLUSIONS AND OUTLOOKS

In this Perspective, we have explored the emerging potential of layered transition metal phosphorus trichalcogenides (MPX_3, where M is a transition metal and X is a chalcogen) as versatile platforms for confined catalysis and energy applications. Drawing inspiration from biological enzymes and established confinement strategies in materials such as zeolites, metal-organic frameworks, carbon nanotubes, and 2D-covered substrates, we introduced the concept of confined reactions, where nanoscale environments alter adsorption energies, charge transfer, and reaction kinetics to enhance selectivity, activity, and stability. We then discussed intercalation as a dynamic tool for modifying layered materials, enabling precise control over electronic,

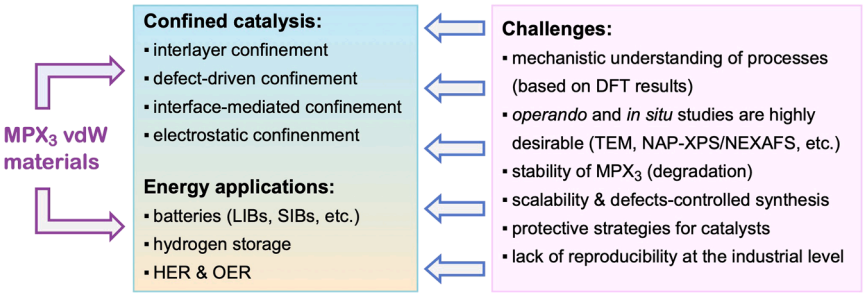

Figure 12. Prospects and challenges of MPX_3 for confined catalysis and energy applications

(Left) Possible applications of MPX_3 in confined catalysis and energy applications (batteries, hydrogen storage, HER, and OER). (Right) Fundamental and technical challenges for the MPX_3 applications.

magnetic, and structural properties through chemical, electrochemical, vapor-phase, and spatially selective methods. This sets the stage for MPX_3 compounds, which exhibit unique bulk properties including tunable band gaps (1.2–3.5 eV), intrinsic magnetic order, and mixed Mott-Hubbard/charge-transfer insulating behavior. These attributes, combined with engineering strategies such as defect creation, alloying, adsorption, and intercalation, position MPX_3 as multifunctional hosts capable of accommodating ions, molecules, and nanoparticles in their vdW gaps.

Building on this foundation, we highlighted MPX_3's role in confined catalysis through multiple modalities: interlayer confinement via intercalants that modulate redox potentials and steric effects; defect-driven confinement, where vacancies and dopants create localized electronic pockets for optimized intermediate binding (e.g., in Co-doped $FePS_3$ for OER); interface-mediated confinement in heterostructures with conductive scaffolds such as defective graphene or N-doped carbon, enhancing charge transport and stability; and electrostatic confinement in amorphous-crystalline junctions (e.g., CoFeB/$NiPS_3$) that generate built-in fields for ampere-level currents. These approaches collectively lower activation barriers and stabilize active sites, as demonstrated in operando studies and DFT calculations for reactions such as HER, OER, and CO_2 reduction.

Finally, we examined MPX_3's applications in energy storage and conversion, including lithium-, sodium-, potassium-, and multivalent-ion batteries, where intercalation and conversion mechanisms yield high capacities and stable cycling when nanoscaled or hybridized. In zinc-air batteries, MPX_3 serves as a bifunctional ORR/OER catalyst, while for hydrogen storage and evolution, defects and substitutions tune adsorption enthalpies toward reversible uptake/release, enabling integrated catalytic-storage systems. Overall, MPX_3 unifies confinement effects with intrinsic catalytic and electronic tunability, offering a pathway to address sustainability challenges in energy technologies.

Despite the promising advancements outlined, several key challenges must be overcome to fully realize the potential of MPX_3 materials in confined catalysis and energy applications (Figure 12). First, mechanistic understanding remains incomplete: while DFT calculations have elucidated adsorption energies and confinement fields in specific systems (e.g., H_2 on vacancy-rich MPX_3), quantitative correlations between structural motifs, such as vacancy density, intercalant size, or interface mismatch, and catalytic free-energy landscapes are limited. *Operando* techniques with atomic resolution, such as *in situ* TEM, ambient-pressure XPS, and synchrotron-based spectroscopies (NEXAFSs), are essential to track dynamic confinement under realistic conditions, but their application to MPX_3 is still nascent. For instance, intercalants may migrate or defects may heal during extended operation, potentially erasing confinement benefits, as seen in early studies of TMDs and MXenes.

Stability represents another critical hurdle. MPX_3 layered structure facilitates intercalation, but also renders them susceptible to degradation in harsh environments, such as acidic/alkaline electrolytes or high temperatures. Vacancy-rich or intercalated phases often exhibit initial high activity, but suffer from capacity fade due to structural reconstruction or side reactions (e.g., polysulfide dissolution in sulfur-based analogs). Enhancing durability requires protective strategies, such as core-shell encapsulation or heterojunctions with stable oxides/phosphides, but these must not compromise accessibility to confined sites. Scalability poses a third challenge: current synthesis methods, including laser ablation, molten-salt intercalation, and solution-based hybridization, are effective at the lab scale, but lack reproducibility for industrial deployment. High-entropy MPX_3 alloys show promise for faster ion diffusion, yet controlling compositional uniformity across large areas remains difficult.

In the short term, prospects may focus on refining existing systems for proof-of-concept devices. For confined catalysis, integrating multiple confinement modes – such as defect-engineered interlayers with electrostatic heterojunctions – could yield hybrid MPX_3 architectures for selective CO_2 reduction or N_2 fixation, building on successes such as $NiPS_3$@DG for pH-universal HER. In energy storage, MPX_3 anodes in sodium- or potassium-ion batteries, paired with scalable cathodes such as $Na_3V_2(PO_4)_3$, may achieve full-cell energy densities >400 W h kg^{-1}, as demonstrated in $FePS_3$@MXene prototypes. Hydrogen applications could see MPX_3 as bifunctional materials in electrolyzers, where tuned vacancies enable HER at low overpotentials (<100 mV) while vdW gaps store H_2 at moderate enthalpies (~20–30 kJ mol^{-1}). Computational screening, leveraging machine learning to predict optimal dopant/vacancy combinations, will accelerate this phase, potentially identifying MPX_3 variants for magnetically modulated catalysis – an underexplored area where spin-charge coupling enhances selectivity.

Medium-term outlooks envision broader integration into sustainable technologies. For confined catalysis, MPX_3 could enable cascade reactions in confined nanoreactors, mimicking enzyme-metal hybrids for efficient biofuel production or pollutant degradation. In batteries, all-solid-state configurations with

MPX_3 electrodes and sulfide electrolytes may surpass liquid-based systems in safety and energy density, addressing electric vehicle demands. Hydrogen prospects include compact storage modules combining MPX_3 sorption with *in situ* HER, suitable for portable power or fuel cells. Cross-disciplinary efforts, such as combining MPX_3 with 2D perovskites or MOFs, could create multifunctional devices for coupled energy conversion-storage. Ultimately, addressing synthesis scalability through vapor-phase or roll-to-roll methods will be pivotal, enabling commercialization. With continued focus on stability and mechanistic insights, MPX_3 holds transformative potential for a hydrogen economy and carbon-neutral energy systems, bridging fundamental science with practical impact.

ACKNOWLEDGMENTS

Y.G. acknowledges the support by the Scientific Research Start-up Fund for High-level Talents of Henan University of Technology (Grant No. 31401823). Y.D. acknowledges the support of the project Centre for Advanced Laser Techniques (CALT), co-funded by the European Union through the European Regional Development Fund under the Competitiveness and Cohesion Operational Programme (Grant No. KK.01.1.1.05.0001). E.V. acknowledges the support of the European Union's NextGenerationEU program. The authors acknowledge financial support from the European Regional Development Fund for the project "Materials for clean energy, advanced sensors and quantum technologies" (Grant No. PK.1.1.10.0002).

AUTHOR CONTRIBUTIONS

Conceptualization, Y.D., Y.G., and E.V.; investigation, Y.D., Y.G., and E.V.; writing – original draft, Y.D., Y.G., and E.V.; writing – review and editing, Y.D., Y.G., and E.V.; funding acquisition, Y.D., Y.G., and E.V.

DECLARATION OF INTERESTS

The authors declare no competing interests.

REFERENCES

1. Yu, S., You, L., and Zhou, S. (2023). A review of optimization modeling and solution methods in renewable energy systems. Front. Eng. Manag. *10*, 640–671. https://doi.org/10.1007/s42524-023-0271-3.
2. Bamisile, O., Cai, D., Adun, H., Dagbasi, M., Ukwuoma, C.C., Huang, Q., Johnson, N., and Bamisile, O. (2024). Towards renewables development: Review of optimization techniques for energy storage and hybrid renewable energy systems. Heliyon *10*, e37482. https://doi.org/10.1016/j.heliyon.2024.e37482.
3. Bernt, M., Hartig-Weiss, A., Tovini, M.F., El-Sayed, H.A., Schramm, C., Schroter, J., Gebauer, C., and Gasteiger, H.A. (2020). Current challenges in catalyst development for PEM water electrolyzers. Chem. Ing. Tech. *92*, 31–39. https://doi.org/10.1002/cite.201900101.
4. Santamaria, L., Lopez, G., Fernandez, E., Cortazar, M., Arregi, A., Olazar, M., and Bilbao, J. (2021). Progress on catalyst development for the steam reforming of biomass and waste plastics pyrolysis volatiles: A review. Energy Fuels. *35*, 17051–17084. https://doi.org/10.1021/acs.energyfuels.1c01666.
5. Yuan, Y., Qi, L., Guo, T., Hu, X., He, Y., and Guo, Q. (2023). A review on the development of catalysts and technologies of CO_2 hydrogenation to produce methanol. Chem. Eng. Commun. *210*, 1791–1821. https://doi.org/10.1080/00986445.2022.2135505.
6. Gonzalez-Granda, S., Albarran-Velo, J., Lavandera, I., and Gotor-Fernandez, V. (2023). Expanding the synthetic toolbox through metal–enzyme cascade reactions. Chem. Rev. *123*, 5297–5346. https://doi.org/10.1021/acs.chemrev.2c00454.
7. Wang, Q., Xing, C., Feng, M., Yang, Y., Pang, D., Feng, X., Zhang, Y., and Wang, B. (2025). Enzyme-assisted confined synthesis of metal nanoparticles in covalent organic frameworks for efficient enzyme-metal cascade catalysis. Angew. Chem. Int. Ed. *64*, e202509105. https://doi.org/10.1002/anie.202509105.
8. Shifa, T.A., and Vomiero, A. (2019). Confined catalysis: progress and prospects in energy conversion. Adv. Energy Mater. *9*, 1902307. https://doi.org/10.1002/aenm.201902307.
9. Guo, C., and Xiao, J. (2019). Towards unifying the concepts of catalysis in confined space. Comput. Mater. Sci. *161*, 58–63. https://doi.org/10.1016/j.commatsci.2019.01.039.
10. Han, X., Gao, Q., Yan, Z., Ji, M., Long, C., and Zhu, H. (2021). Electrocatalysis in confined spaces: interplay between well-defined materials and the microenvironment. Nanoscale *13*, 1515–1528. https://doi.org/10.1039/d0nr08237f.
11. Mao, Y., Zuo, W., Wu, C., Ma, W., Tian, Y., Zhang, J., Li, L., Zhan, W., and Qiu, J. (2025). Advances and challenges in the application of confined catalysts in heterogeneous advanced oxidation processes: A review. J. Clean. Prod. *491*, 144762. https://doi.org/10.1016/j.jclepro.2025.144762.
12. Dou, X., Yan, T., Li, W., Zhu, C., Chen, T., Lo, B.T.W., Marini, C., Xiao, H., and Liu, L. (2025). Structure–reactivity relationship of zeolite-confined Rh catalysts for hydroformylation of linear α-olefins. J. Am. Chem. Soc. *147*, 2726–2736. https://doi.org/10.1021/jacs.4c15445.
13. Chai, Y., Dai, W., Wu, G., Guan, N., and Li, L. (2021). Confinement in a zeolite and zeolite catalysis. Acc. Chem. Res. *54*, 2894–2904. https://doi.org/10.1021/acs.accounts.1c00274.
14. Pan, X., and Bao, X. (2011). The effects of confinement inside carbon nanotubes on catalysis. Acc. Chem. Res. *44*, 553–562. https://doi.org/10.1021/ar100160t.
15. Xiao, J., Zhao, M., Wang, Y., and Zhang, X. (2017). Excitons in atomically thin 2D semiconductors and their applications. Nanophotonics *6*, 1309–1328. https://doi.org/10.1515/nanoph-2016-0160.
16. Li, H., Xiao, J., Fu, Q., and Bao, X. (2017). Confined catalysis under two-dimensional materials. Proc. Natl. Acad. Sci. USA *114*, 5930–5934. https://doi.org/10.1073/pnas.1701280114.
17. Wei, F., Wan, Q., Lin, S., and Guo, H. (2020). Origin of confined catalysis in nanoscale reactors between two-dimensional covers and metal substrates: Mechanical or electronic? J. Phys. Chem. C *124*, 11564–11573. https://doi.org/10.1021/acs.jpcc.0c03621.
18. Zhou, Y., Chen, W., Cui, P., Zeng, J., Lin, Z., Kaxiras, E., and Zhang, Z. (2016). Enhancing the hydrogen activation reactivity of nonprecious metal substrates via confined catalysis underneath graphene. Nano Lett. *16*, 6058–6063. https://doi.org/10.1021/acs.nanolett.6b02052.
19. Li, H., Guo, C., Fu, Q., and Xiao, J. (2019). Toward fundamentals of confined electrocatalysis in nanoscale reactors. J. Phys. Chem. Lett. *10*, 533–539. https://doi.org/10.1021/acs.jpclett.8b03448.
20. Tian, H., Yang, H., Liu, X., Jia, Y., and Xu, Q. (2025). Confinement effect on the electrochemical CO_2 reduction reaction. Green Chem. *27*, 1238–1253. https://doi.org/10.1039/d4gc05274a.
21. Fan, X., Li, D., Shu, Y., Feng, Y., and Li, F. (2024). Confinement effect and application in catalytic oxidation–reduction reaction of confined single-atom catalysts. ACS Catal. *14*, 12991–13014. https://doi.org/10.1021/acscatal.4c02113.
22. Chen, Z., Kirlikovali, K.O., Idrees, K.B., Wasson, M.C., and Farha, O.K. (2022). Porous materials for hydrogen storage. Chem *8*, 693–716. https://doi.org/10.1016/j.chempr.2022.01.012.
23. Chen, L., Ting, V.P., Zhang, Y., Coventry, J., Rahbari, A., Yin, Z., Wang, F., Tian, M., Rochat, S., Zhang, Z., et al. (2025). Hydrate-based H_2 storage with porous materials as heterogeneous promoters: state of

the art and challenges. J. Mater. Chem. A *13*, 27001–27049. https://doi.org/10.1039/d5ta04503g.

24. Ghotia, S., Kumar, P., and Srivastava, A.K. (2025). A review on 2D materials: unveiling next-generation hydrogen storage solutions, advancements and prospects. J. Mater. Sci. *60*, 1071–1097. https://doi.org/10.1007/s10853-024-10054-3.
25. Zhang, Q., Qiao, Z., Cao, X., Qu, B., Yuan, J., Fan, T.E., Zheng, H., Cui, J., Wu, S., Xie, Q., and Peng, D.L. (2020). Rational integration of spatial confinement and polysulfide conversion catalysts for high sulfur loading lithium–sulfur batteries. Nanoscale Horiz. *5*, 720–729. https://doi.org/10.1039/c9nh00663j.
26. Lateef, S.A., Manjum, M., McRay, H.A., Mustain, W.E., and Jalilvand, G. (2023). Self-structured binder confinement of sulfur for highly durable lithium-sulfur batteries. ACS Appl. Energy Mater. *6*, 9307–9317. https://doi.org/10.1021/acsaem.3c01205.
27. Yari, S., Conde Reis, A., Pang, Q., and Safari, M. (2025). Performance benchmarking and analysis of lithium-sulfur batteries for next-generation cell design. Nat. Commun. *16*, 5473. https://doi.org/10.1038/s41467-025-60528-4.
28. Susner, M.A., Chyasnavichyus, M., McGuire, M.A., Ganesh, P., and Maksymovych, P. (2017). Metal thio- and selenophosphates as multifunctional van der Waals layered materials. Adv. Mater. *29*, 1602852. https://doi.org/10.1002/adma.201602852.
29. Zhu, M., Kou, H., Wang, K., Wu, H., Ding, D., Zhou, G., and Ding, S. (2020). Promising functional two-dimensional lamellar metal thiophosphates: synthesis strategies, properties and applications. Mater. Horiz. *7*, 3131–3160. https://doi.org/10.1039/d0mh00802h.
30. Zhang, H., Wei, T., Qiu, Y., Zhang, S., Liu, Q., Hu, G., Luo, J., and Liu, X. (2023). Recent progress in metal phosphorous chalcogenides: Potential high-performance electrocatalysts. Small *19*, e2207249. https://doi.org/10.1002/smll.202207249.
31. Dedkov, Y., Guo, Y., and Voloshina, E. (2023). Progress in the studies of electronic and magnetic properties of layered MPX_3 materials (M: transition metal, X: chalcogen). Electron. Struct. *5*, 043001. https://doi.org/10.1088/2516-1075/acfa4e.
32. Pramoda, K., and Rao, C.N.R. (2023). 2D transition metal based phosphochalcogenides and their applications in photocatalytic and electrocatalytic hydrogen evolution reactions. J. Mater. Chem. A. *11*, 16933–16962. https://doi.org/10.1039/d3ta01629c.
33. Wang, H., Cheng, P., Wu, B., Yan, Y., Schaaf, P., Sofer, Z., and Wang, D. (2024). 2D metal phosphorous trichalcogenides (MPCh 3) for sustainable energy storage and conversion: Nanoarchitectonics and advanced applications. Adv. Funct. Mater. *34*, 2407432. https://doi.org/10.1002/adfm.202407432.
34. Dedkov, Y., and Voloshina, E. (2025). Beyond pristine layers: Engineering van der Waals MPX_3 materials (M: transition metal, X: chalcogen) via defects, adsorption, and intercalation. Small Sci. *5*, 2500307. https://doi.org/10.1002/smsc.202500307.
35. Boscoboinik, J.A. (2019). Chemistry in confined space through the eyes of surface science – 2D porous materials. J. Phys. Condens. Matter *31*, 063001. https://doi.org/10.1088/1361-648x/aaf2ce.
36. Mezenov, Y.A., Bruyere, S., Krasilin, A., Khrapova, E., Bachinin, S.V., Alekseevskiy, P.V., Shipiloskikh, S., Boulet, P., Hupont, S., Nomine, A., et al. (2022). Insights into solid-to-solid transformation of MOF amorphous phases. Inorg. Chem. *61*, 13992–14003. https://doi.org/10.1021/acs.inorgchem.2c01978.
37. Zhao, T., Huang, X., Cui, R., Han, W., Zhang, G., and Tang, Z. (2023). Design of confined catalysts and applications in environmental catalysis: Original perspectives and further prospects. J. Clean. Prod. *390*, 136125. https://doi.org/10.1016/j.jclepro.2023.136125.
38. Zhestkij, N.A., Efimova, A.S., Kenzhebayeva, Y., Dmitriev, M.V., Novikov, A.S., Yushina, I.D., Krylov, A., Timofeeva, M.V., Kulakova, A.N., Glebova, N.V., et al. (2023). Nonlinear metal-organic framework crystals for efficient multicolor coherent optical emission. Adv. Opt. Mater. *11*, 2300881. https://doi.org/10.1002/adom.202300881.
39. Bachinin, S.V., Marunchenko, A., Matchenya, I., Zhestkij, N., Shirobokov, V., Gunina, E., Novikov, A., Timofeeva, M., Povarov, S.A., Li, F., and Milichko, V.A. (2024). Metal-organic framework single crystal for in-memory neuromorphic computing with a light control. Commun. Mater. *5*, 128. https://doi.org/10.1038/s43246-024-00573-6.
40. Luo, Y., Li, X., Cai, X., Zou, X., Kang, F., Cheng, H.M., and Liu, B. (2018). Two-dimensional MoS_2 confined $Co(OH)_2$ electrocatalysts for hydrogen evolution in alkaline electrolytes. ACS Nano *12*, 4565–4573. https://doi.org/10.1021/acsnano.8b00942.
41. Mashtalir, O., Naguib, M., Mochalin, V.N., Dall'Agnese, Y., Heon, M., Barsoum, M.W., and Gogotsi, Y. (2013). Intercalation and delamination of layered carbides and carbonitrides. Nat. Commun. *4*, 1716. https://doi.org/10.1038/ncomms2664.
42. Pazek, S., Efimenko, A., Felix, R., Roslova, M., Querebillo, C.J., Gorbunov, M.V., Ovchinnikov, A., Koitzsch, A., Escudero, C., Shemerliuk, Y., et al. (2024). Charge compensation in a layered van der Waals $NiPS_3$ host through various cationic intercalations. J. Mater. Chem. A *12*, 3523–3541. https://doi.org/10.1039/d3ta06196e.
43. Gu, Q., Lu, M., Cao, Y., and Zhang, B. (2023). Revealing the catalytic conversion via in situ characterization for lithium–sulfur batteries. Renewables *1*, 601–621. https://doi.org/10.31635/rnwb.023.202300033.
44. Liu, Z., Tee, S.Y., Guan, G., and Han, M.Y. (2024). Atomically substitutional engineering of transition metal dichalcogenide layers for enhancing tailored properties and superior applications. Nano-Micro Lett. *16*, 95. https://doi.org/10.1007/s40820-023-01315-y.
45. Gu, Q., Cao, Y., Chen, J., Qi, Y., Zhai, Z., Lu, M., Huang, N., and Zhang, B. (2024). Fluorine-modulated MXene-derived catalysts for multiphase sulfur conversion in lithium–sulfur battery. Nano-Micro Lett. *16*, 266. https://doi.org/10.1007/s40820-024-01482-6.
46. Wang, W., Shan, Q., Xu, J., Li, H., Wang, Y., Hao, R., Wan, X., Zhao, C., and Wang, W. (2026). Theoretical design rules for the reconstruction of transition metal sulfides during oxygen evolution reactions. J. Energy Chem. *112*, 317–328. https://doi.org/10.1016/j.jechem.2025.08.049.
47. Munoz-Santiburcio, D., Wittekindt, C., and Marx, D. (2013). Nanoconfinement effects on hydrated excess protons in layered materials. Nat. Commun. *4*, 2349. https://doi.org/10.1038/ncomms3349.
48. Mu, R., Fu, Q., Jin, L., Yu, L., Fang, G., Tan, D., and Bao, X. (2012). Visualizing chemical reactions confined under graphene. Angew. Chem. Int. Ed. *51*, 4856–4859. https://doi.org/10.1002/anie.201200413.
49. Zhang, X., Cui, H., Zhang, J., and Tang, J. (2017). Adsorption characteristic of Pd-4 cluster carbon nanotube towards transformer oil dissolved components: A simulation. Appl. Surf. Sci. *419*, 802–810. https://doi.org/10.1016/j.apsusc.2017.05.004.
50. Zhao, Q., Buongiorno Nardelli, M., Lu, W., and Bernholc, J. (2005). Carbon nanotube-metal cluster composites: A new road to chemical sensors? Nano Lett. *5*, 847–851. https://doi.org/10.1021/nl050167w.
51. Duchene, N.A., and Rochefort, A. (2019). Quantum size effects of Ag_n clusters on carbon nanotubes. J. Phys. Chem. C *123*, 28769–28776. https://doi.org/10.1021/acs.jpcc.9b08690.
52. Shafiee, A., Rabiee, N., Ahmadi, S., Baneshi, M., Khatami, M., Iravani, S., and Varma, R.S. (2022). Core-shell nanophotocatalysts: Review of materials and applications. ACS Appl. Nano Mater. *5*, 55–86. https://doi.org/10.1021/acsanm.1c03714.
53. Si, M., Lin, F., Ni, H., Wang, S., Lu, Y., and Meng, X. (2023). Research progress of yolk-shell structured nanoparticles and their application in catalysis. RSC Adv. *13*, 2140–2154. https://doi.org/10.1039/d2ra07541e.
54. Dresselhaus, M.S., and Dresselhaus, G. (2002). Intercalation compounds of graphite. Adv. Phys. X. *51*, 1–186. https://doi.org/10.1080/00018730110113644.
55. Rajapakse, M., Karki, B., Abu, U.O., Pishgar, S., Musa, M.R.K., Riyadh, S.M.S., Yu, M., Sumanasekera, G., and Jasinski, J.B. (2021). Intercalation

as a versatile tool for fabrication, property tuning, and phase transitions in 2D materials. npj 2D Mater. Appl. *5*, 30. https://doi.org/10.1038/s41699-021-00211-6.

56. Odetallah, M., and Kuss, C. (2023). A review of chemically induced intercalation and deintercalation in battery materials. Energy Tech. *11*, 2201060. https://doi.org/10.1002/ente.202201060.

57. Yang, R., Mei, L., Lin, Z., Fan, Y., Lim, J., Guo, J., Liu, Y., Shin, H.S., Voiry, D., Lu, Q., et al. (2024). Intercalation in 2D materials and in situ studies. Nat. Rev. Chem *8*, 410–432. https://doi.org/10.1038/s41570-024-00605-2.

58. Liu, Y., Wang, Z., Hu, G., Chen, X., Xu, K., Guo, Y., Xie, Y., and Wu, C. (2025). Precision intercalation of organic molecules in 2D layered materials: From interface chemistry to low-dimensional physics. Precis. Chem. *3*, 51–71. https://doi.org/10.1021/prechem.4c00084.

59. Li, N., Sun, M.Z., Hwang, S., Li, S., Zhao, H.Y., Du, Y.P., Huang, B.L., and Su, D. (2021). Non-equilibrium insertion of lithium ions into graphite. J. Mater. Chem. A *9*, 12080–12086. https://doi.org/10.1039/d1ta02836g.

60. Caffrey, N.M., Johansson, L.I., Xia, C., Armiento, R., Abrikosov, I.A., and Jacobi, C. (2016). Structural and electronic properties of Li-intercalated graphene on SiC(0001). Phys. Rev. B *93*, 195421. https://doi.org/10.1103/physrevb.93.195421.

61. Masse, R.C., Liu, C., Li, Y., Mai, L., and Cao, G. (2017). Energy storage through intercalation reactions: Electrodes for rechargeable batteries. Natl. Sci. Rev. *4*, 26–53. https://doi.org/10.1093/nsr/nww093.

62. Chen, B., Hope-Glenn, N., Wright, A., Messinger, R.J., and Couzis, A. (2025). Mechanistic understanding of lithium-ion adsorption, intercalation, and plating during charging of graphite electrodes. ACS Electrochem. *1*, 574–587. https://doi.org/10.1021/acselectrochem.4c00079.

63. Zhan, D., Sun, L., Ni, Z.H., Liu, L., Fan, X.F., Wang, Y., Yu, T., Lam, Y.M., Huang, W., and Shen, Z.X. (2010). $FeCl_3$-based few-layer graphene intercalation compounds: Single linear dispersion electronic band structure and strong charge transfer doping. Adv. Funct. Mater. *20*, 3504–3509. https://doi.org/10.1002/adfm.201000641.

64. Zhao, W., Tan, P.H., Liu, J., and Ferrari, A.C. (2011). Intercalation of few-layer graphite flakes with $FeCl_3$: Raman determination of Fermi level, layer by layer decoupling, and stability. J. Am. Chem. Soc. *133*, 5941–5946. https://doi.org/10.1021/ja110939a.

65. Cai, X., Luo, Y., Liu, B., and Cheng, H.M. (2018). Preparation of 2D material dispersions and their applications. Chem. Soc. Rev. *47*, 6224–6266. https://doi.org/10.1039/c8cs00254a.

66. Raza, A., Hassan, J.Z., Ikram, M., Ali, S., Farooq, U., Khan, Q., and Maqbool, M. (2021). Advances in liquid-phase and intercalation exfoliations of transition metal dichalcogenides to produce 2D framework. Adv. Mater. Interfaces *8*, 2002205. https://doi.org/10.1002/admi.202002205.

67. Huang, Q., Li, X., Sun, M., Zhang, L., Song, C., Zhu, L., Chen, P., Xu, Z., Wang, W., and Bai, X. (2017). The mechanistic insights into the 2H-1T phase transition of MoS_2 upon alkali metal intercalation: from the study of dynamic sodiation processes of MoS_2 nanosheets. Adv. Mater. Interfaces *4*, 1700171. https://doi.org/10.1002/admi.201700171.

68. Jin, Q., Liu, N., Chen, B., and Mei, D. (2018). Mechanisms of semiconducting 2H to metallic 1T phase transition in two-dimensional MoS_2 nanosheets. J. Phys. Chem. C *122*, 28215–28224. https://doi.org/10.1021/acs.jpcc.8b10256.

69. Wang, Z., Li, R., Su, C., and Loh, K.P. (2020). Intercalated phases of transition metal dichalcogenides. SmartMat. *1*, e1013. https://doi.org/10.1002/smm2.1013.

70. Fujimoto, H., Yamaki, T., Shimoda, K., Fujinami, S., Nakatani, T., Kano, G., Kawasaki, M., Ogumi, Z., and Abe, T. (2022). Phase diagram of Li-graphite intercalation compound formed by the charge/discharge reaction in Li-ion battery. J. Electrochem. Soc. *169*, 070507. https://doi.org/10.1149/1945-7111/ac7e77.

71. Hazrati, E., de Wijs, G.A., and Brocks, G. (2014). Li intercalation in graphite: A van der Waals density-functional study. Phys. Rev. B *90*, 155448. https://doi.org/10.1103/physrevb.90.155448.

72. Emery, N., Hérold, C., dAstuto, M., Garcia, V., Bellin, C., Marêché, J.F., Lagrange, P., and Loupias, G. (2005). Superconductivity of bulk CaC_6. Phys. Rev. Lett. *95*, 087003. https://doi.org/10.1103/physrevlett.95.087003.

73. Weller, T.E., Ellerby, M., Saxena, S.S., Smith, R.P., and Skipper, N.T. (2005). Superconductivity in the intercalated graphite compounds C_6Yb and C_6Ca. Nat. Phys. *1*, 39–41. https://doi.org/10.1038/nphys0010.

74. Hart, J.L., Hantanasirisakul, K., Lang, A.C., Anasori, B., Pinto, D., Pivak, Y., van Omme, J.T., May, S.J., Gogotsi, Y., and Taheri, M.L. (2019). Control of MXenes' electronic properties through termination and intercalation. Nat. Commun. *10*, 522. https://doi.org/10.1038/s41467-018-08169-8.

75. Li, J., Wang, H., and Xiao, X. (2020). Intercalation in two-dimensional transition metal carbides and nitrides (MXenes) toward electrochemical capacitor and beyond. Energy Environ. Mater. *3*, 306–322. https://doi.org/10.1002/eem2.12090.

76. Voloshina, E.N., and Dedkov, Y.S. (2014). Electronic and magnetic properties of the graphene/Eu/Ni(111) hybrid system. Z. Naturforsch. *69*, 297–302. https://doi.org/10.5560/zna.2014-0012.

77. Jugovac, M., Cojocariu, I., Sánchez-Barriga, J., Gargiani, P., Valvidares, M., Feyer, V., Blügel, S., Bihlmayer, G., and Perna, P. (2023). Inducing single spin-polarized flat bands in monolayer graphene. Adv. Mater. *35*, e2301441. https://doi.org/10.1002/adma.202301441.

78. Sheverdyaeva, P.M., Bihlmayer, G., Cappelluti, E., Pacilé, D., Mazzola, F., Atodiresei, N., Jugovac, M., Grimaldi, I., Contini, G., Kundu, A.K., et al. (2024). Spin-gependent $\pi\pi^*$gap in graphene on a magnetic substrate. Phys. Rev. Lett. *132*, 266401. https://doi.org/10.1103/physrevlett.132.266401.

79. Voloshina, E., Schiller, F., Ali, K., Mohammed Idris Bakhit, A., Castrillo-Bodero, R., Paulus, B., and Dedkov, Y. (2025). Europium intercalation as a route to modulate electronic and magnetic properties of *h*-BN/Ni(111). Nanoscale *17*, 25071–25080. https://doi.org/10.1039/d5nr03875h.

80. Duong, D.L., Yun, S.J., and Lee, Y.H. (2017). Van der Waals layered materials: Opportunities and challenges. ACS Nano *11*, 11803–11830. https://doi.org/10.1021/acsnano.7b07436.

81. Liao, L., Kovalska, E., Regner, J., Song, Q., and Sofer, Z. (2024). Two-dimensional van der Waals thin film and device. Small *20*, e2303638. https://doi.org/10.1002/smll.202303638.

82. Tezze, D., Pereira, J.M., Asensio, Y., Ipatov, M., Calavalle, F., Casanova, F., Bittner, A.M., Ormaza, M., Martín-García, B., Hueso, L.E., and Gobbi, M. (2022). Tuning the magnetic properties of $NiPS_3$ through organic-ion intercalation. Nanoscale *14*, 1165–1173. https://doi.org/10.1039/d1nr07281a.

83. Basnet, R., and Hu, J. (2024). Understanding and tuning magnetism in van der Waals-type metal thiophosphates. Nanoscale *16*, 15851–15883. https://doi.org/10.1039/d4nr01577k.

84. Zaanen, J., Sawatzky, G.A., and Allen, J.W. (1985). Band gaps and electronic structure of transition-metal compounds. Phys. Rev. Lett. *55*, 418–421. https://doi.org/10.1103/physrevlett.55.418.

85. Yang, J., Zhou, Y., Guo, Q., Dedkov, Y., and Voloshina, E. (2020). Electronic, magnetic and optical properties of $MnPX_3$ (X = S, Se) monolayers with and without chalcogen defects: A first-principles study. RSC Adv. *10*, 851–864. https://doi.org/10.1039/c9ra09030d.

86. Kamata, A., Noguchi, K., Suzuki, K., Tezuka, H., Kashiwakura, T., Ohno, Y., and Nakai, S.i. (1997). Resonant 2p→3 dphotoemission measurement of MPS_3 (M = Mn, Fe, Ni). J. Phys. Soc. Jpn. *66*, 401–407. https://doi.org/10.1143/jpsj.66.401.

87. Strasdas, J., Pestka, B., Rybak, M., Budniak, A.K., Leuth, N., Boban, H., Feyer, V., Cojocariu, I., Baranowski, D., Avila, J., et al. (2023). Electronic

band structure changes across the antiferromagnetic phase transition of exfoliated $MnPS_3$ flakes probed by μ-ARPES. Nano Lett. *23*, 10342–10349. https://doi.org/10.1021/acs.nanolett.3c02906.

88. Jin, Y., Yan, M., Kremer, T., Voloshina, E., and Dedkov, Y. (2022). Mott-Hubbard insulating state for the layered van der Waals $FePX_3$ (X: S, Se) as revealed by NEXAFS and resonant photoelectron spectroscopy. Sci. Rep. *12*, 735. https://doi.org/10.1038/s41598-021-04557-1.

89. Yan, M., Jin, Y., Voloshina, E., and Dedkov, Y. (2023). Electronic correlations in Fe_xNiyPS_3 van der Waals materials: Insights from angle-resolved photoelectron spectroscopy and DFT. J. Phys. Chem. Lett. *14*, 9774–9779. https://doi.org/10.1021/acs.jpclett.3c02688.

90. Yan, M., Jin, Y., Wu, Z., Tsaturyan, A., Makarova, A., Smirnov, D., Voloshina, E., and Dedkov, Y. (2021). Correlations in the electronic structure of van der Waals $NiPS_3$ crystals: An x-ray absorption and resonant photoelectron spectroscopy study. J. Phys. Chem. Lett. *12*, 2400–2405. https://doi.org/10.1021/acs.jpclett.1c00394.

91. Klaproth, T., Aswartham, S., Shemerliuk, Y., Selter, S., Janson, O., van den Brink, J., Büchner, B., Knupfer, M., Pazek, S., Mikhailova, D., et al. (2023). Origin of the magnetic exciton in the van der Waals antiferromagnet $NiPS_3$. Phys. Rev. Lett. *131*, 256504. https://doi.org/10.1103/physrevlett.131.256504.

92. Jin, Y., Jin, Y., Li, K., Yan, M., Guo, Y., Zhou, Y., Preobrajenski, A., Dedkov, Y., and Voloshina, E. (2022). Mixed insulating state for van der Waals $CoPS_3$. J. Phys. Chem. Lett. *13*, 10486–10493. https://doi.org/10.1021/acs.jpclett.2c02992.

93. Fonin, M., Enenkel, V., Rakic, I.S., Dedkov, Y., and Voloshina, E. (2025). Orbital analysis of electronic states for vdW material $CoPS_3$ by scanning probe microscopy. J. Phys. Chem. C *129*, 5762–5768. https://doi.org/10.1021/acs.jpcc.5c00330.

94. Bai, W., Hu, Z., Xiao, C., Guo, J., Li, Z., Zou, Y., Liu, X., Zhao, J., Tong, W., Yan, W., et al. (2020). Parasitic ferromagnetism in few-layered transition-metal chalcogenophosphate. J. Am. Chem. Soc. *142*, 10849–10855. https://doi.org/10.1021/jacs.0c04101.

95. Koster, J., Storm, A., Ghorbani-Asl, M., Kretschmer, S., Gorelik, T.E., Krasheninnikov, A.V., and Kaiser, U. (2022). Structural and chemical modifications of few-layer transition metal phosphorous trisulfides by electron irradiation. J. Phys. Chem. C *126*, 15446–15455. https://doi.org/10.1021/acs.jpcc.2c03800.

96. Storm, A., Koster, J., Ghorbani-Asl, M., Kretschmer, S., Gorelik, T.E., Krasheninnikov, A.V., and Kaiser, U. (2023). Structural transformations in few-layer $MnPSe_3$ stimulated by thermal annealing and electron irradiation. J. Phys. Chem. C *127*, 24713–24723. https://doi.org/10.1021/acs.jpcc.3c07112.

97. Storm, A., Köster, J., Ghorbani-Asl, M., Kretschmer, S., Gorelik, T.E., Kinyanjui, M.K., Krasheninnikov, A.V., and Kaiser, U. (2023). Electron-beam- and thermal-annealing-induced structural transformations in few-layer $MnPS_3$. ACS Nano *17*, 4250–4260. https://doi.org/10.1021/acsnano.2c05895.

98. Wang, F., Mathur, N., Janes, A.N., Sheng, H., He, P., Zheng, X., Yu, P., DeRuiter, A.J., Schmidt, J.R., He, J., and Jin, S. (2021). Defect-mediated ferromagnetism in correlated two-dimensional transition metal phosphorus trisulfides. Sci. Adv. *7*, eabj4086. https://doi.org/10.1126/sciadv.abj4086.

99. Li, K., Yan, M., Jin, Y., Jin, Y., Guo, Y., Voloshina, E., and Dedkov, Y. (2023). Dual character of the insulating state in the van der Waals $Fe_{1-x}Ni_xPS_3$ alloyed compounds. J. Phys. Chem. Lett. *14*, 57–65. https://doi.org/10.1021/acs.jpclett.2c03492.

100. Huang, S., Qiu, Z., Zhong, J., Wu, S., Han, X., Hu, W., Han, Z., Cheng, W.N., Luo, Y., Meng, Y., et al. (2024). High-entropy transition metal phosphorus trichalcogenides for rapid sodium ion diffusion. Adv. Mater. *36*, e2405170. https://doi.org/10.1002/adma.202405170.

101. Guo, Y., Cai, G., Zhou, J., Yang, J., Voloshina, E., and Dedkov, Y. (2024). XPS analysis of $Fe_xNi_yPS_3$ vdW materials used in the hydrogen evolution processes. ChemPhysChem *25*, e202400039. https://doi.org/10.1002/cphc.202400039.

102. Wu, Z., Xu, S., Zhou, Y., Guo, Q., Dedkov, Y., and Voloshina, E. (2021). Adsorption of water molecules on pristine and defective $NiPX_3$ (X: S, Se) monolayers. Adv. Theory Simul. *4*, 2100182. https://doi.org/10.1002/adts.202100182.

103. Xu, S., Wu, Z., Dedkov, Y., and Voloshina, E. (2021). Adsorption of water on the pristine and defective semiconducting 2D $CrPX_3$ monolayers (X: S, Se). J. Phys. Condens. Matter *33*, 354001. https://doi.org/10.1088/1361-648x/ac0ab4.

104. Dai, J., Wang, K., Voloshina, E., Dedkov, Y., and Paulus, B. (2023). Probing active sites on pristine and defective $MnPX_3$ (X: S and Se) monolayers for electrocatalytic water splitting. ACS Omega *8*, 33920–33927. https://doi.org/10.1021/acsomega.3c04677.

105. Kumar, R., Jenjeti, R.N., and Sampath, S. (2020). Two-dimensional, few-layer $MnPS_3$ for selective NO_2 gas sensing under ambient conditions. ACS Sens. *5*, 404–411. https://doi.org/10.1021/acssensors.9b02064.

106. Kumar, R., Jenjeti, R.N., Choutipalli, V.S.K., Subramanian, V., and Sampath, S. (2021). Conductometric NO_x sensor based on exfoliated two-dimensional layered $MnPSe_3$. Sens. Actuators B: Chem. *347*, 130633. https://doi.org/10.1016/j.snb.2021.130633.

107. Ji, L., Chang, L., Zhang, Y., Mou, S., Wang, T., Luo, Y., Wang, Z., and Sun, X. (2019). Electrocatalytic CO_2 reduction to alcohols with high selectivity over a two-dimensional $Fe_2P_2S_6$ nanosheet. ACS Catal. *9*, 9721–9725. https://doi.org/10.1021/acscatal.9b03180.

108. Grasso, V., and Silipigni, L. (2002). Low-dimensional materials: The MPX_3 family, physical features and potential future applications. Riv. Nuovo Cim. *25*, 1–102. https://doi.org/10.1007/bf03548909.

109. Jin, Y., Yan, M., Dedkov, Y., and Voloshina, E. (2022). Realization of the electric-field driven one-material-based magnetic tunnel junction using van der Waals antiferromagnetic $MnPX_3$ (X: S, Se). J. Mater. Chem. C *10*, 3812–3818. https://doi.org/10.1039/d1tc05922j.

110. Tezze, D., Pereira, J.M., Tutar, D., Ramos, M., Regner, J., Gargiani, P., Schiller, F., Casanova, F., Alegria, A., Martín-García, B., et al. (2024). Tunable magnetism in 2D organic-ion-intercalated $MnPS_3$ via molecule-dependent vacancy generation. Adv. Funct. Mater. *35*, 2412771. https://doi.org/10.1002/adfm.202412771.

111. Ou, Y., Li, X., Kopaczek, J., Davis, A., Jackson, G., Sayyad, M., Liu, F., and Tongay, S.A. (2024). The hard ferromagnetism in $FePS_3$ induced by non-magnetic molecular intercalation. Adv. Phys. Res *4*, 2400101. https://doi.org/10.1002/apxr.202400101.

112. Zhang, X., Zhao, X., Wu, D., Jing, Y., and Zhou, Z. (2016). $MnPSe_3$ monolayer: A promising 2D visible-light photohydrolytic catalyst with high carrier mobility. Adv. Sci. *3*, 1600062. https://doi.org/10.1002/advs.201600062.

113. Gusmão, R., Sofer, Z., and Pumera, M. (2019). Metal phosphorous trichalcogenides ($MPCh_3$): From synthesis to contemporary energy challenges. Angew. Chem., Int. Ed. *58*, 9326–9337. https://doi.org/10.1002/anie.201810309.

114. Zhang, X., Zhou, H., Su, X., Chen, X., Yang, C., Qin, J., and Inokuchi, M. (2007). Synthesis, characterization and magnetic properties of transition metal salen complexes intercalated into layered $MnPS_3$. J. Alloys Compd. *432*, 247–252. https://doi.org/10.1016/j.jallcom.2006.05.107.

115. Xu, R., Fu, G., Ding, W., Li, Y., Yang, G., Yu, P., Li, S., and Liu, P. (2025). Laser-induced Co-doped $FePS_3$ with massively phosphorus sulfur vacancies nanosheet for efficient and highly stable electrocatalytic oxygen reaction. Adv. Sci. *12*, 2501836. https://doi.org/10.1002/advs.202501836.

116. Yu, J., Li, W.J., Zhang, H., Zhou, F., Li, R., Xu, C.Y., Zhou, L., Zhong, H., and Wang, J. (2019). Metallic $FePSe_3$ nanoparticles anchored on N-doped carbon framework for All-*p*H hydrogen evolution reaction. Nano Energy *57*, 222–229. https://doi.org/10.1016/j.nanoen.2018.12.055.

117. Tong, Y., Chen, P., Chen, L., and Cui, X. (2021). Dual vacancies confined in nickel phosphosulfide nanosheets enabling robust overall water splitting. ChemSusChem *14*, 2576–2584. https://doi.org/10.1002/cssc.202100720.

118. Zhang, J., Cui, R., Li, X., Liu, X., and Huang, W. (2017). A nanohybrid consisting of $NiPS_3$ nanoparticles coupled with defective graphene as a *p*H-universal electrocatalyst for efficient hydrogen evolution. J. Mater. Chem. A *5*, 23536–23542. https://doi.org/10.1039/c7ta07672j.

119. Zhao, S., Liu, Y., Chen, Y., Li, L., Zhai, W., Guo, Z., and Dai, Z. (2024). Amorphous-crystalline CoFeB/$NiPS_3$ vertical heterostructure with a built-in electric field for robust ampere-level water oxidation. J. Mater. Chem. A *12*, 10704–10712. https://doi.org/10.1039/d4ta01168f.

120. Zhang, H., Meng, G., Liu, Q., Luo, Y., Niederberger, M., Feng, L., Luo, J., and Liu, X. (2023). Metal phosphorous chalcogenide: A promising material for advanced energy storage systems. Small *19*, e2303165. https://doi.org/10.1002/smll.202303165.

121. Samal, R., Sanyal, G., Chakraborty, B., and Rout, C.S. (2021). Two-dimensional transition metal phosphorous trichalcogenides (MPX_3): a review on emerging trends, current state and future perspectives. J. Mater. Chem. A *9*, 2560–2591. https://doi.org/10.1039/d0ta09752g.

122. Gui, Q., Feng, Y., Chen, B., Gu, F., Chen, L., Meng, S., Xu, M., Xia, M., Zhang, C., and Yang, J. (2021). Extrinsic-structured bimetallic-phase ternary metal phosphorus trisulfides coupled with N-doped graphitized carbon for superior electrochemical lithium storage. Adv. Energy Mater. *11*, 2003553. https://doi.org/10.1002/aenm.202003553.

123. Huang, Y.F., Yang, Y.C., and Tuan, H.Y. (2023). Construction of strongly coupled few-layer $FePSe_3$-CNT hybrids for high performance potassium-ion storage devices. Chem. Eng. J. *451*, 139013. https://doi.org/10.1016/j.cej.2022.139013.

124. Hao, Y., Huang, A., Han, S., Huang, H., Song, J., Sun, X., Wang, Z., Li, L., Hu, F., Xue, J., and Peng, S. (2020). Plasma-treated ultrathin ternary $FePSe_3$ nanosheets as a bifunctional electrocatalyst for efficient zinc-air batteries. ACS Appl. Mater. Interfaces *12*, 29393–29403. https://doi.org/10.1021/acsami.0c08133.

125. Wang, M., Han, J., Liu, W., Kamiko, M., and Yagi, S. (2021). Energy storage mechanism of monocrystalline layered $FePS_3$ and $FePSe_3$ as active materials for Mg batteries and pseudocapacitors. J. Alloys Compd. *883*, 160822. https://doi.org/10.1016/j.jallcom.2021.160822.

126. Shen, H., Cai, Y., Ma, Z., Wang, P., Guo, B., Cheng, J., Li, Q., Wang, H., Liu, Z., Nie, A., and Wu, J. (2023). Layered manganese phosphorus trisulfides for high-performance lithium-ion batteries and the storage mechanism. Carbon Energy *5*, e290. https://doi.org/10.1002/cey2.290.

127. Ding, Y., Chen, Y., Xu, N., Lian, X., Li, L., Hu, Y., and Peng, S. (2020). Facile synthesis of $FePS_3$ nanosheets@MXene composite as a high-performance anode material for sodium storage. Nano-Micro Lett. *12*, 54. https://doi.org/10.1007/s40820-020-0381-y.

128. Liang, Q., Zheng, Y., Du, C., Luo, Y., Zhang, J., Li, B., Zong, Y., and Yan, Q. (2017). General and scalable solid-state synthesis of 2D MPS_3 (M = Fe, Co, Ni) nanosheets and tuning their Li/Na storage properties. Small Methods *1*, 1700304. https://doi.org/10.1002/smtd.201700304.

129. Zhong, L., Chen, H., Xie, W., Jia, W., Xiao, Y., Cheng, B., Lin, L., and Lei, S. (2024). Intercalation and defect engineering of layered $MnPS_3$ for greatly enhanced capacity and stability in sodium-ion batteries. Chem. Eng. J. *481*, 148370. https://doi.org/10.1016/j.cej.2023.148370.

130. Zheng, J., Wu, Y., Sun, Y., Rong, J., Li, H., and Niu, L. (2020). Advanced anode materials of potassium ion batteries: From zero dimension to three dimensions. Nano-Micro Lett. *13*, 12. https://doi.org/10.1007/s40820-020-00541-y.

131. Chen, B.C., Lu, X., Zhong, H.Y., Huang, P.W., Wu, Y.N., Xu, S.Y., Du, K.Z., and Wu, X.H. (2022). Constructing $FePSe_3$– $FeSe_2$ heterojunctions uniformly in a Ketjen black carbon matrix for superior potassium ion batteries. J. Mater. Chem. A *10*, 25671–25682. https://doi.org/10.1039/d2ta07426e.

132. Fujii, Y., Miura, A., Rosero-Navarro, N.C., Higuchi, M., and Tadanaga, K. (2017). $FePS_3$ electrodes in all-solid-state lithium secondary batteries using sulfide-based solid electrolytes. Electrochim. Acta *241*, 370–374. https://doi.org/10.1016/j.electacta.2017.04.089.

133. Wang, T., Shi, Z., Wang, F., He, J., Zhong, Y., Ma, Y., Zhu, Z., Cheng, X.B., Ozoemena, K.I., and Wu, Y. (2024). Advanced bifunctional catalyst design for rechargeable zinc-air batteries. EES Catal. *2*, 696–726. https://doi.org/10.1039/d4ey00014e.

134. Ye, C., Xu, S., Li, H., Shan, J., and Qiao, S.Z. (2025). Developing cathode films for practical all-solid-state lithium-sulfur batteries. Adv. Mater. *37*, 2407738. https://doi.org/10.1002/adma.202407738.

135. Mukherjee, D., Austeria, P.M., and Sampath, S. (2016). Two-dimensional, few-layer phosphochalcogenide, $FePS_3$: a new catalyst for electrochemical hydrogen evolution over wide pH range. ACS Energy Lett. *1*, 367–372. https://doi.org/10.1021/acsenergylett.6b00184.

136. Ismail, N., El-Meligi, A.A., Temerk, Y.M., and Madian, M. (2010). Synthesis and characterization of layered $FePS_3$ for hydrogen uptake. Int. J. Hydrogen Energy *35*, 7827–7834. https://doi.org/10.1016/j.ijhydene.2010.05.061.

137. Ismail, N., Madian, M., and El-Meligi, A.A. (2014). Synthesis of $NiPS_3$ and CoPS and its hydrogen storage capacity. J. Alloys Compd. *588*, 573–577. https://doi.org/10.1016/j.jallcom.2013.11.073.

138. Cabria, I., and El-Meligi, A.A. (2018). DFT simulation of hydrogen storage on manganese phosphorous trisulphide ($MnPS_3$). Int. J. Hydrogen Energy *43*, 5903–5912. https://doi.org/10.1016/j.ijhydene.2017.10.103.

139. Wang, S., Xiao, B., Shen, S., Song, K., Lin, Z., Wang, Z., Chen, Y., and Zhong, W. (2020). Cobalt doping of $FePS_3$ promotes intrinsic active sites for the efficient hydrogen evolution reaction. Nanoscale *12*, 14459–14464. https://doi.org/10.1039/d0nr03819a.

140. Wert, S., Iffelsberger, C., Padinjareveetil, A.K.K., and Pumera, M. (2023). Edges of layered $FePSe_3$ exhibit increased electrochemical and electrocatalytic activity compared to basal planes. ACS Appl. Electron. Mater. *5*, 928–934. https://doi.org/10.1021/acsaelm.2c01493.

141. Mahamiya, V., Shukla, A., Adak, A.K., Lee, H., Seriani, N., and Gebauer, R. (2025). Computational simulations and strategies for optimal hydrogen storage materials design. PRX Energy *4*, 022001. https://doi.org/10.1103/prxenergy.4.022001.

142. Ao, Z.M., and Peeters, F.M. (2010). High-capacity hydrogen storage in Al-adsorbed graphene. Phys. Rev. B *81*, 205406. https://doi.org/10.1103/physrevb.81.205406.